

Supporting material for:

UV-light promoted C–H bond activation of benzene and fluorobenzenes by an iridium(I) pincer complex

Simone A. Hauser, Jack Emerson-King, Scott Habershon, and Adrian B. Chaplin*

Department of Chemistry, University of Warwick, Gibbet Hill Road, Coventry CV4 7AL, UK.

E-mail: a.b.chaplin@warwick.ac.uk

Contents

1	Synthetic details	2
1.1	General experimental methods	2
1.1.1	Selected data for [Ir(2,6-(P ^t Bu ₂ CH ₂) ₂ C ₆ H ₃)(CO)] (1).....	3
1.2	General procedure for photolysis experiments	4
1.2.1	Photolysis of 1 in C ₆ D ₆	5
1.2.2	Photolysis of 2 in C ₆ D ₆	5
1.2.3	Photolysis of 1 in C ₆ H ₅ F.....	6
1.2.4	Photolysis of 1 in 1,2-C ₆ H ₄ F ₂	6
1.2.5	Photolysis of 1 in 1,3,5-C ₆ H ₃ F ₃	7
1.3	General procedure for the preparation of [Ir(2,6-(P^tBu₂CH₂)₂C₆H₃)(Ar)H(CO)] (2 and 3)	7
1.3.1	[Ir(2,6-(P ^t Bu ₂ CH ₂) ₂ C ₆ H ₃)(C ₆ H ₅)H(CO)] (2).....	7
1.3.2	[Ir(2,6-(P ^t Bu ₂ CH ₂) ₂ C ₆ H ₃)(2-C ₆ H ₄ F)H(CO)] (3a).....	10
1.3.3	[Ir(2,6-(P ^t Bu ₂ CH ₂) ₂ C ₆ H ₃)(2,3-C ₆ H ₃ F ₂)H(CO)] (3b).....	12
1.3.4	[Ir(2,6-(P ^t Bu ₂ CH ₂) ₂ C ₆ H ₃)(2,4,6-C ₆ H ₂ F ₃)H(CO)] (3c).....	16
1.4	Crystallography	19
2	Computational details	20
2.1	Geometry optimisations and free energy calculations.....	20
2.2	Infrared vibrational modes.....	23
2.3	TD-DFT calculations and assignment of UV-vis spectra.....	24
3	References	39

1 Synthetic details

1.1 General experimental methods

All manipulations were performed under an atmosphere of argon, using Schlenk and glove box techniques. Glassware was oven dried at 150 °C overnight and flamed under vacuum prior to use. Anhydrous heptane and benzene (<0.005% H₂O) were purchased from ACROS or Aldrich and freeze-pump-thaw degassed three times before being placed under argon. C₆D₆ and C₆D₁₂ were dried over sodium and vacuum distilled. Fluoroarenes (C₆H₅F, 1,2-C₆H₄F₂, 1,3,5-C₆H₃F₃) were dried over CaH₂, vacuum distilled and stored over thoroughly vacuum-dried 3 Å molecular sieves. [Ir(2,6-(P^tBu₂CH₂)₂C₆H₃)(CO)] (**1**) was prepared using an adapted literature protocol.¹ [Ir(2,6-(P^tBu₂CH₂)₂C₆H₃)HCl]² was prepared from [Ir(COD)Cl]₂³ and 1,3-(P^tBu₂CH₂)₂C₆H₄² in an analogous procedure to structurally related [Ir(2,6-(P^tBu₂O)₂C₆H₃)HCl].⁴ All other solvents and reagents are commercial products and were used as received. NMR spectra were recorded on Bruker AV spectrometers at 298 K unless otherwise stated. NMR spectra recorded in fluoroarenes were locked and referenced using an internal sealed capillary of C₆D₆. Chemical shifts are quoted in ppm and coupling constants in Hz. IR spectra were recorded on a PerkinElmer Spectrum One FT-IR spectrometer at 293 K. UV-Vis spectra were recorded on an Agilent Technologies Cary 60 UV-vis spectrometer at 293 K. Microanalyses were performed by Stephen Boyer at London Metropolitan University.

1.1.1 Selected data for $[\text{Ir}(\text{2,6-}(\text{P}^t\text{Bu}_2\text{CH}_2)_2\text{C}_6\text{H}_3)(\text{CO})]$ (**1**)

$^{31}\text{P}\{^1\text{H}\}$ NMR (C_6D_6 , 202 MHz): δ 82.0 (s). $^{31}\text{P}\{^1\text{H}\}$ NMR (C_6D_{12} , 202 MHz): δ 81.8 (s).

IR (C_6H_{12}): $\nu(\text{CO}) = 1926.8 \text{ cm}^{-1}$.

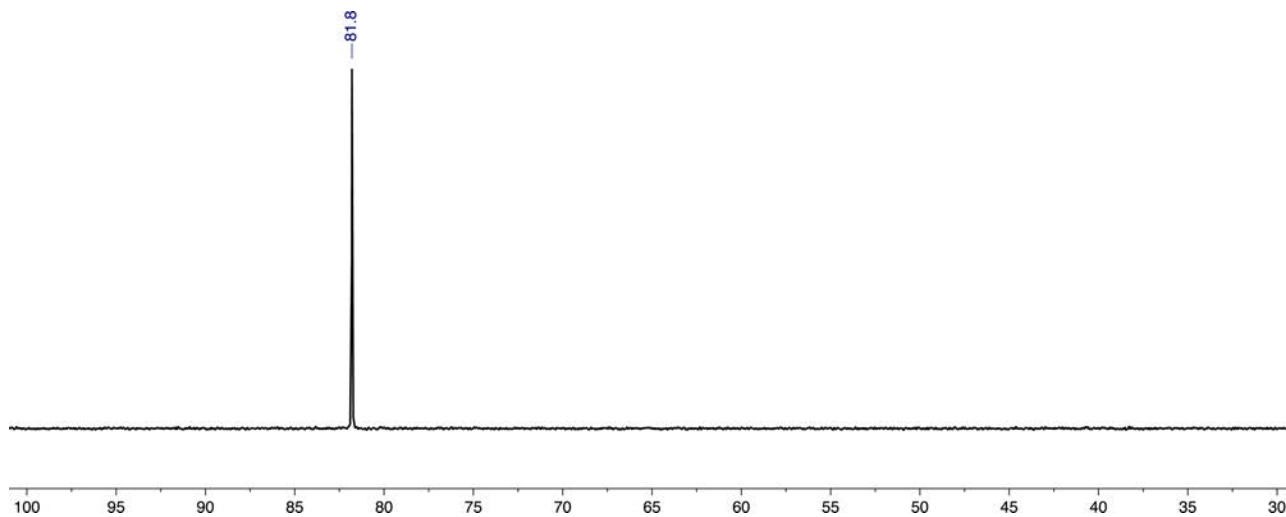


Figure S-1: $^{31}\text{P}\{^1\text{H}\}$ NMR spectrum of **1** (C_6D_{12} , 202 MHz).

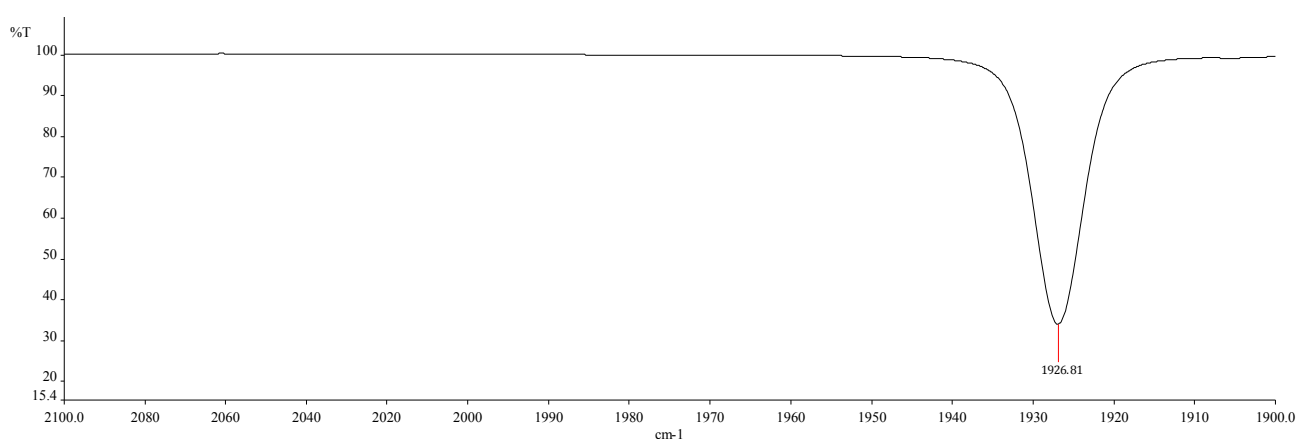


Figure S-2: Carbonyl stretching band in the IR spectrum of **1** (C_6H_{12}).

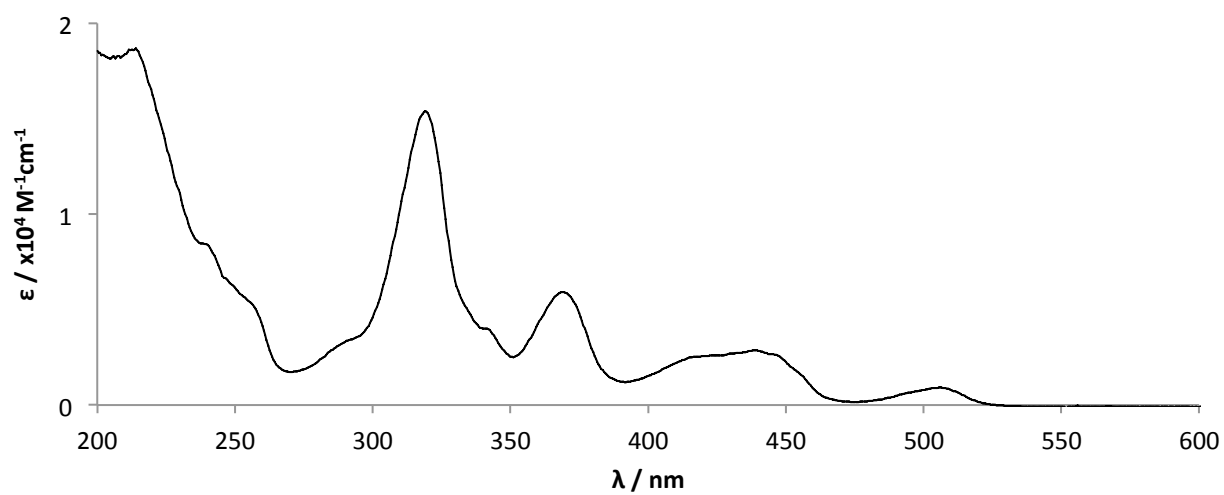


Figure S-3: UV-vis spectrum of **1** (C_6H_{12}).

1.2 General procedure for photolysis experiments

A solution of iridium pincer (0.01 mmol) in arene (0.5 mL) in a 5 mm quartz J. Young's NMR tube under argon was irradiated using a 100 W Hg arc lamp equipped with a water IR filter (Figure S-4). Reaction progress was monitored by ^1H and ^{31}P NMR spectroscopy.



Figure S-4: Photolysis equipment (100 W Hg arc lamp): power supply (a), arc lamp (b), safety shutter and IR filter (c), interlocked reaction chamber (d), quartz NMR tubes held in beam (e).

1.2.1 Photolysis of 1 in C₆D₆

Following the general procedure, the **1:2-d₆** ratio observed by ³¹P{¹H} NMR spectroscopy after 3 hours total irradiation was 1:1.63.

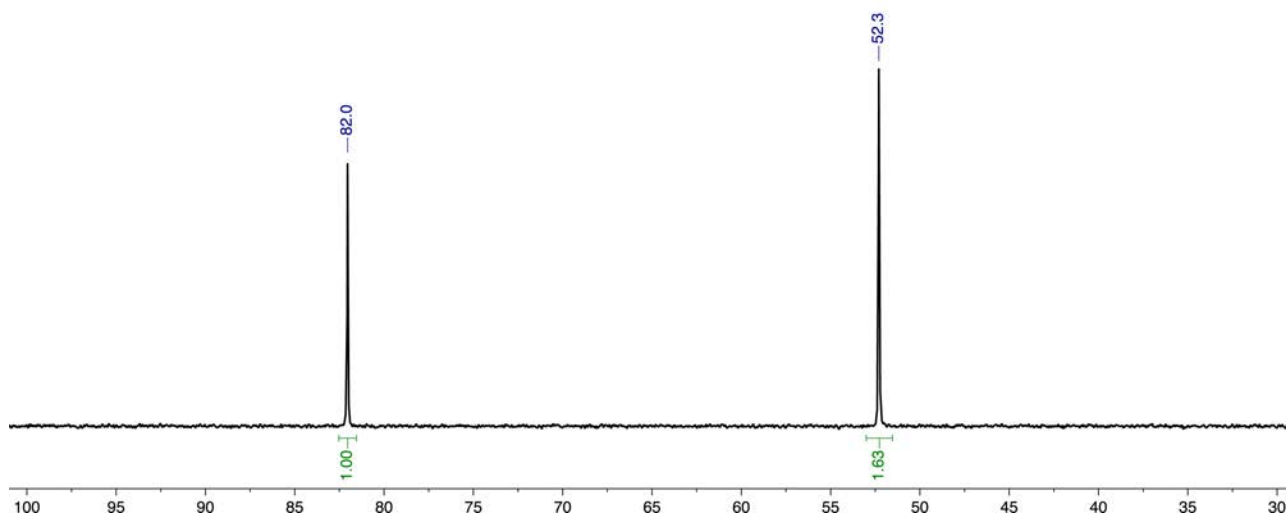


Figure S-5: ³¹P{¹H} NMR spectrum of **1** after 3 hours total irradiation in C₆D₆ (202 MHz).

1.2.2 Photolysis of 2 in C₆D₆

Following the general procedure, the **1:2-d₆** ratio observed by ³¹P{¹H} NMR spectroscopy after 3 hours total irradiation was 1:1.64.

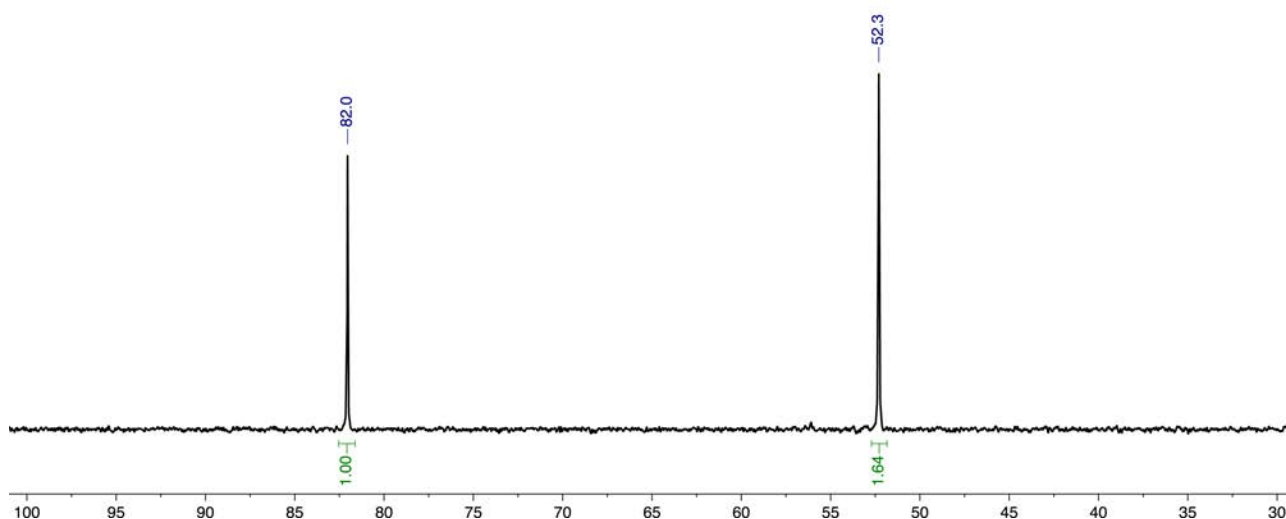


Figure S-6: ³¹P{¹H} NMR spectrum of **2** after 3 hours total irradiation in C₆D₆ (202 MHz).

1.2.3 Photolysis of **1** in C₆H₅F

Following the general procedure, the **1:3a** ratio observed by ³¹P{¹H} NMR spectroscopy after 8 hours total irradiation was 1:8.96.

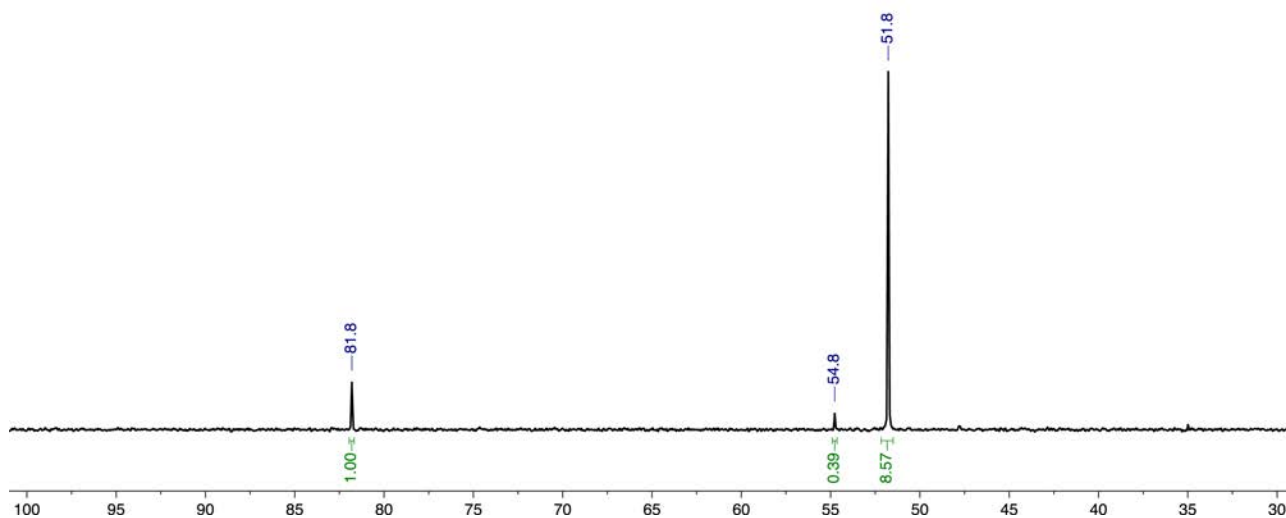


Figure S-7: ³¹P{¹H} NMR spectrum of **1** after 8 hours total irradiation in C₆H₅F (202 MHz).

1.2.4 Photolysis of **1** in 1,2-C₆H₄F₂

Following the general procedure, the **1:3b** ratio observed by ³¹P{¹H} NMR spectroscopy after 8 hours total irradiation was 1:3.13. Irradiation is accompanied by formation of a small amount of unknown compound at δ 67.9 (3% total by integration) that we attribute to reaction of {Ir(PCP)} with a trace impurity in the solvent (*ca* 60 ppm). The total conversion to **3b** was 74%.

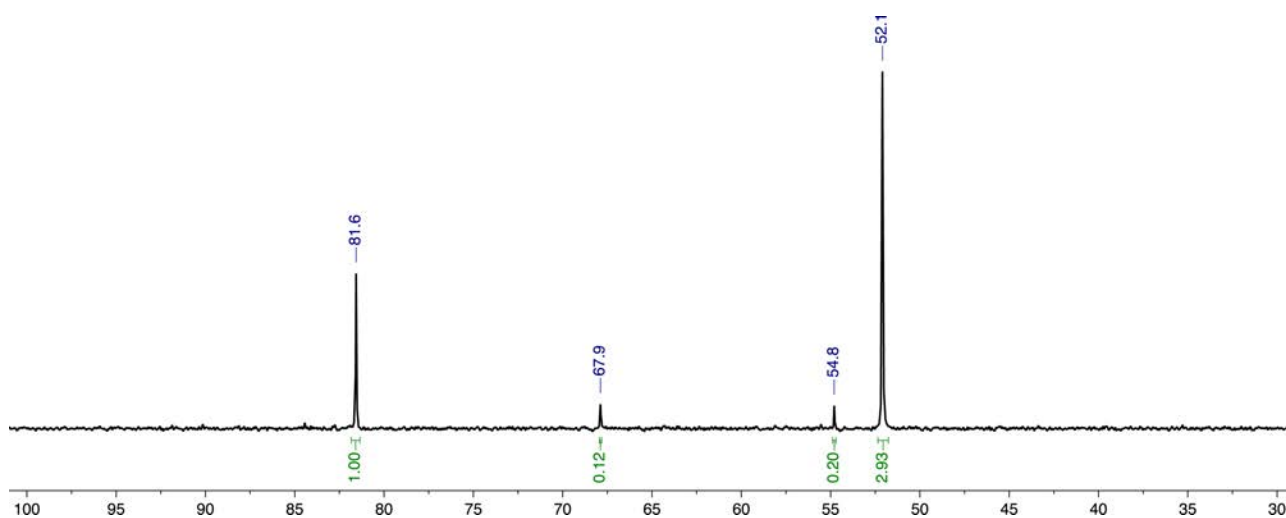


Figure S-8: ³¹P{¹H} NMR spectrum of **1** after 8 hours total irradiation in 1,2-C₆H₄F₂ (162 MHz).

1.2.5 Photolysis of **1** in 1,3,5-C₆H₃F₃

Following the general procedure, the **1:3c** ratio observed by ³¹P{¹H} NMR spectroscopy after 8 hours total irradiation was 1:2.91.

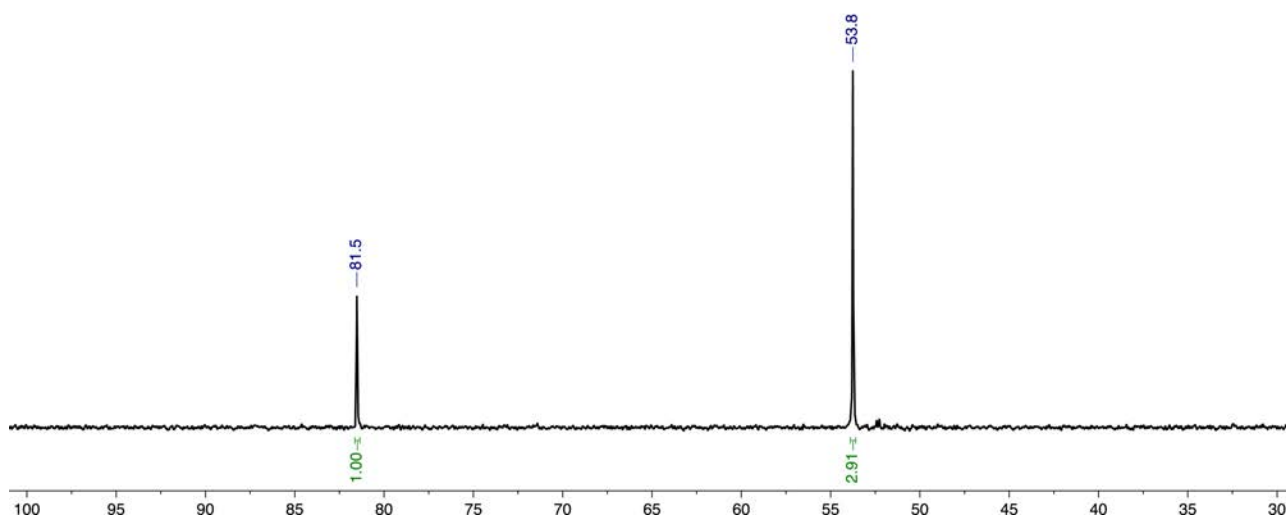


Figure S-8: ³¹P{¹H} NMR spectrum of **1** after 8 hours total irradiation in 1,3,5-C₆H₃F₃ (202 MHz).

1.3 General procedure for the preparation of [Ir(2,6-(P^tBu₂CH₂)₂C₆H₃)(Ar)H(CO)] (**2** and **3**)

A suspension of [Ir(2,6-(P^tBu₂CH₂)₂C₆H₃)Cl] (*ca* 0.05 mol, 1 equiv.), K[O^tBu] (1.1 equiv.) in arene (*ca* 5 mL, excess) was heated at 75°C for 30 minutes. The solution was cooled to 0°C and placed under CO (1 atm) and stirred at room temperature for 1 hour. The volatiles were removed *in vacuo* and residue extracted with heptane. Cooling the filtrate to -20°C afforded analytically pure crystalline products.

1.3.1 [Ir(2,6-(P^tBu₂CH₂)₂C₆H₃)(C₆H₅)H(CO)] (**2**)

Prepared using the general procedure. Yield = 54%.

Single crystalline sample for analysis by X-ray diffraction grown from heptane at -20 °C (Figure S-35).

Spectroscopic data is in agreement with literature values, but we report a more comprehensive characterisation below.⁵

¹H NMR (C₆D₁₂, 500 MHz): δ 7.95 (d, ³J_{HH} = 7.4, 1H, Ph), 7.86 (d, ³J_{HH} = 6.6, 1H, Ph), 6.86 (d, ³J_{HH} = 7.5, 2H, C₆H₃), 6.74 – 6.79 (m, 1H, Ph), 6.72 (t, ³J_{HH} = 7.5, 1H, C₆H₃), 6.67 – 6.70 (m, 2H, Ph), 3.46 (dt, ²J_{HH} = 16.1, J_{PH} = 4.1, 2H, CH₂), 3.39 (dt, ²J_{HH} = 16.1, J_{PH} = 3.3, 2H, CH₂), 1.20 (t, J_{PH} = 6.6, 18H, ^tBu), 1.17 (t, J_{PH} = 6.6, 18H, ^tBu), -9.07 (t, ³J_{PH} = 17.6, 1H, IrH).

¹³C{¹H} NMR (C₆D₁₂, 126 MHz): δ 184.0 (m, CO), 150.4 (s, C₆H₃{IrC}), 148.7 (s, Ph), 148.2 (t, J_{PC} = 6, C₆H₃{CCH₂}), 147.7 (s, Ph), 133.8 (t, ²J_{PC} = 7, Ph{IrC}), 128.2 (s, Ph), 127.1 (s, Ph), 124.4 (s, C₆H₃), 121.3 (s, Ph), 120.6 (t, J_{PC} = 7, C₆H₃), 42.9 (t, J_{PC} = 15, CH₂), 37.5 (t, J_{PC} = 10, ^tBu{C}), 37.4 (t, J_{PC} = 13, ^tBu{C}), 30.1 (s, ^tBu{Me}), 29.9 (s, ^tBu{Me}).

$^{31}\text{P}\{^1\text{H}\}$ NMR (C_6D_{12} , 202 MHz): δ 51.1 (s). $^{31}\text{P}\{^1\text{H}\}$ NMR (C_6D_6 , 202 MHz): δ 52.3 (s).

IR (C_6H_{12}): $\nu(\text{CO}) = 1981.7, 1971.1 \text{ cm}^{-1}$.

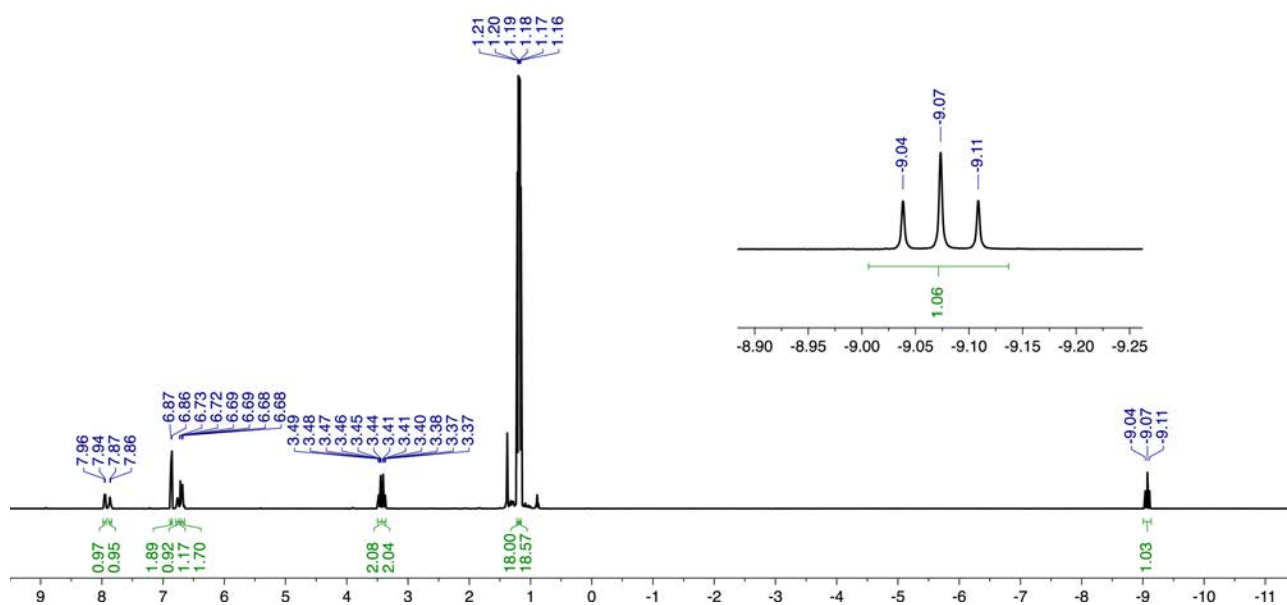


Figure S-9: ^1H NMR spectrum of **2** (C_6D_{12} , 500 MHz).

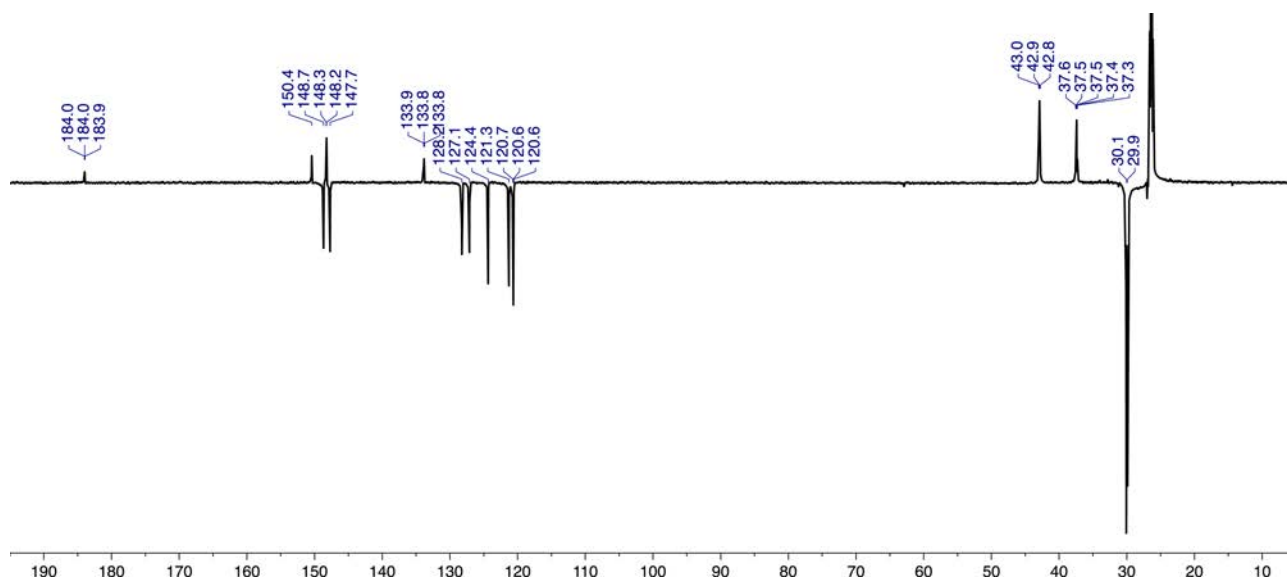


Figure S-10: $^{13}\text{C}\{^1\text{H}\}$ APT NMR spectrum of **2** (C_6D_{12} , 126 MHz).

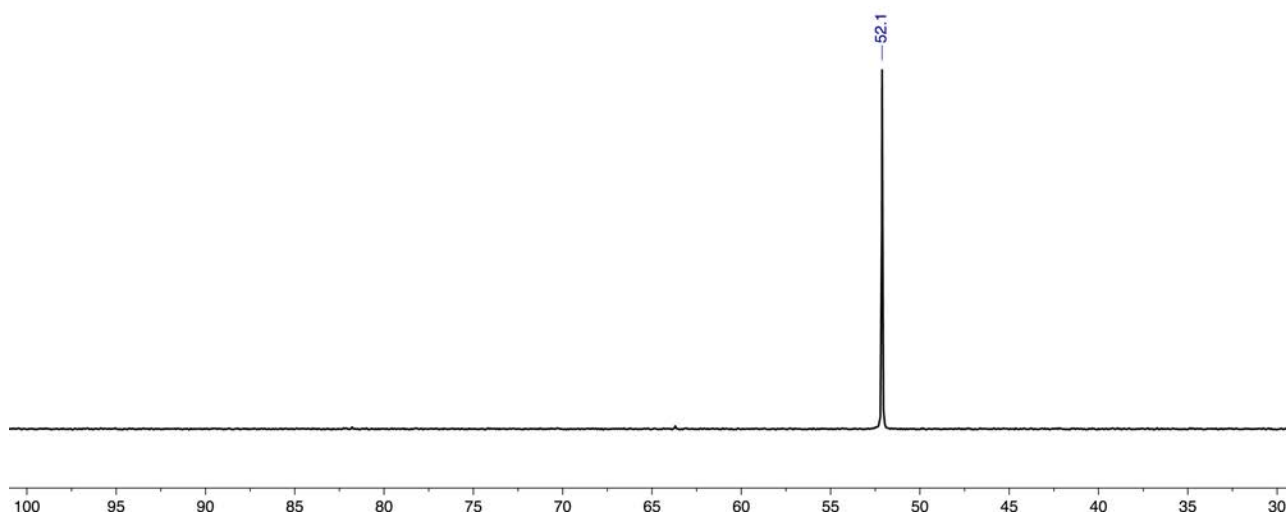


Figure S-11: $^{31}\text{P}\{^1\text{H}\}$ NMR spectrum of **2** (C_6D_{12} , 202 MHz).

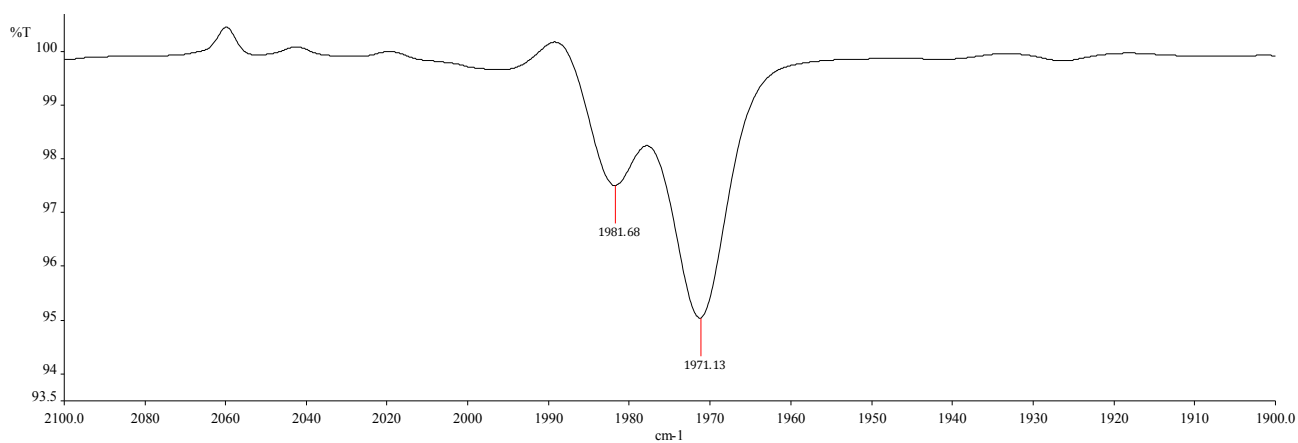


Figure S-12: Carbonyl stretching bands in the IR spectrum of **2** (C_6H_{12}).

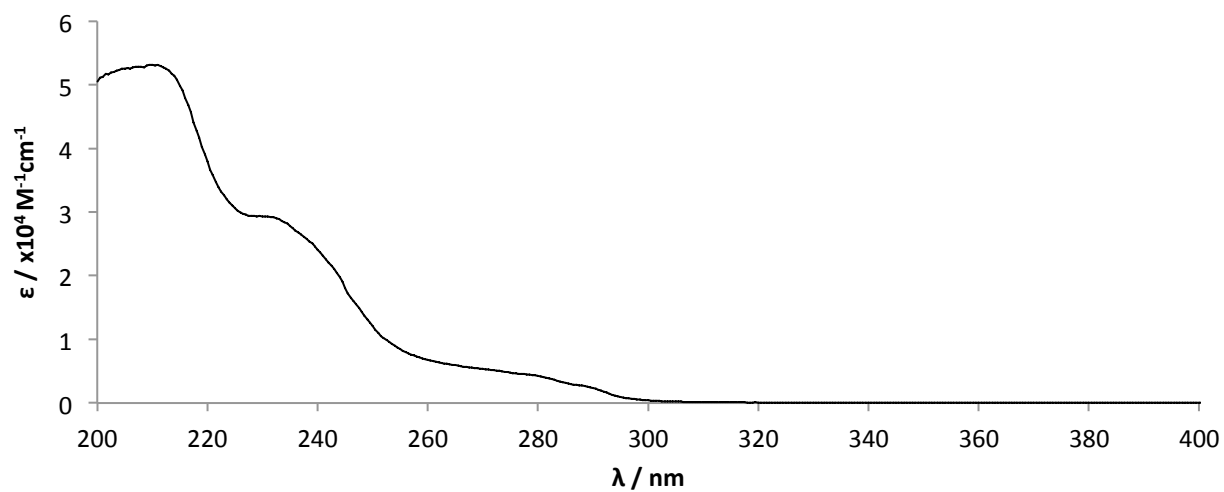


Figure S-11: UV-vis spectrum of **2** (C_6H_{12})

1.3.2 [Ir(2,6-(P^tBu₂CH₂)₂C₆H₃)(2-C₆H₄F)H(CO)] (3a)

Prepared using the general procedure. Yield = 32%.

Single crystalline sample for analysis by X-ray diffraction grown from heptane at -20 °C (Figure S-36).

Assignment of the rotamers was achieved by detection of an NOE interaction for Ir-H...H-Ar^F(C6) in the major rotamer (Figure S-18). This interaction is absent in the minor rotamer and instead ^{1h}J_{FH} coupling of 10.0 Hz for the Ir-H resonance is observed (cf. 10.8 for **3c**).

¹H NMR (C₆D₁₂, 500 MHz, major rotamer): δ 7.94 (app. t, *J* = 6, 1H, Ar^F), 6.87 (d, ³J_{HH} = 7.5, 2H, C₆H₃), 6.73 (t, ³J_{HH} = 7.5, 1H, C₆H₃), 6.68 – 6.72 (m, 2H, Ar^F), 6.49 – 6.53 (m, 1H, Ar^F), 3.43 (dt, ²J_{HH} = 16.0, *J*_{PH} = 4.0, 2H, CH₂), 3.38 (dt, ²J_{HH} = 16.1, *J*_{PH} = 3.3, 2H, CH₂), 1.18 (t, *J*_{PH} = 6.5, 18H, ^tBu), 1.17 (t, *J*_{PH} = 6.5, 18H, ^tBu), -9.68 (td, ³J_{PH} = 17.2, ⁴J_{FH} = 2.4, 1H, IrH). ¹H NMR (C₆D₁₂, 500 MHz, selected data for minor rotamer): δ 8.07 (app. t, *J* = 6, 1H, Ar^F), -8.86 (td, ³J_{PH} = 17.2, ^{1h}J_{FH} = 10.0, 1H, IrH).

¹³C{¹H} NMR (C₆D₁₂, 126 MHz, major rotamer): δ 181.5 (m, CO), 169.5 (d, ¹J_{FC} = 227, Ar^F), 151.1 (d, ³J_{FC} = 17, Ar^F), 148.9 (d, *J* = 4, C₆H₃{IrC}), 148.2 (t, *J*_{PC} = 6, C₆H₃{CCH₂}), 124.4 (s, C₆H₃), 123.9 (d, ³J_{FC} = 9, Ar^F), 123.3 (s, Ar^F), 120.9 (t, *J*_{PC} = 7, C₆H₃), 119.7 (dt, ²J_{FC} = 47, ²J_{PC} = 7, Ar^F{IrC}), 113.1 (d, ²J_{FC} = 35, Ar^F), 42.1 (t, *J*_{PC} = 15, CH₂), 37.5 (t, *J*_{PC} = 13, ^tBu{C}), 36.6 (t, *J*_{PC} = 10, ^tBu{C}), 30.1 (s, ^tBu{Me}), 29.8 (s, ^tBu{Me}).

¹⁹F{¹H} NMR (C₆D₁₂, 377 MHz): δ -71.48 (s, minor rotamer), -72.71 (s, major rotamer).

³¹P{¹H} NMR (C₆D₁₂, 202 MHz): δ 54.5 (s, minor rotamer), 51.7 (s, major rotamer). ³¹P{¹H} NMR (C₆H₅F/C₆D₆, 202 MHz): δ 54.8 (s, minor rotamer), 51.8 (s, major rotamer).

Anal. Calcd. for C₃₁H₄₈IrOP₂ (709.89 g·mol⁻¹): C, 52.45; H, 6.82; N, 0.00. Found: C, 52.37; H, 6.66; N, 0.00.

IR (C₆H₁₂): ν(CO) = 1987.7, 1997.9 cm⁻¹.

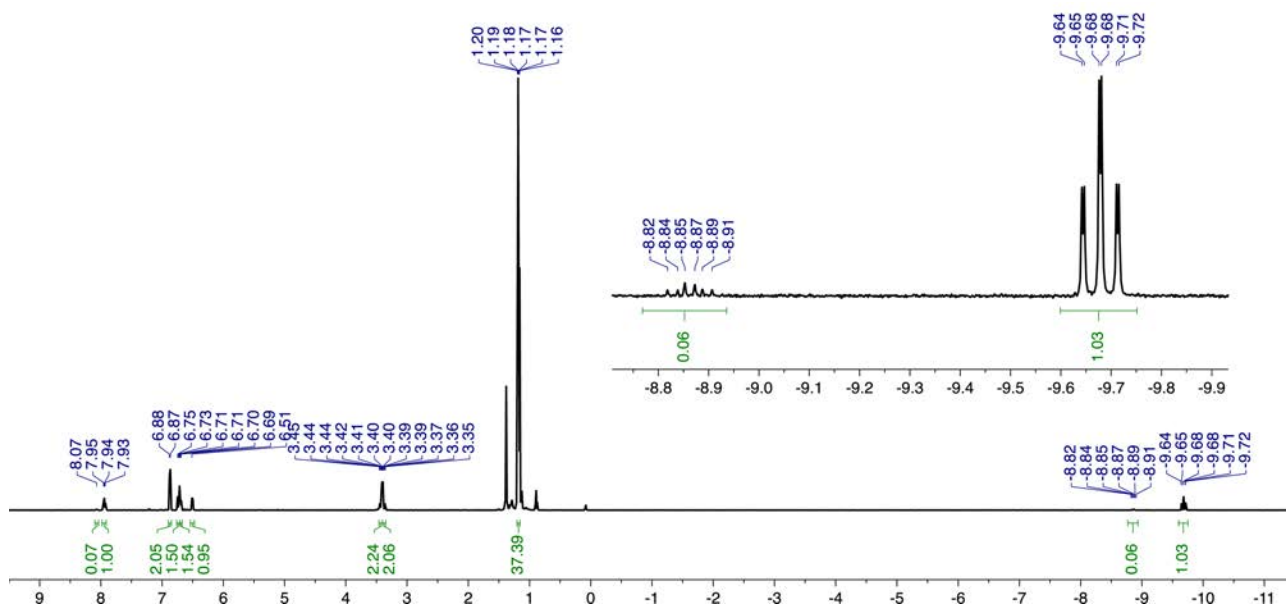


Figure S-14: ¹H NMR spectrum of **3a** (C₆D₁₂, 500 MHz).

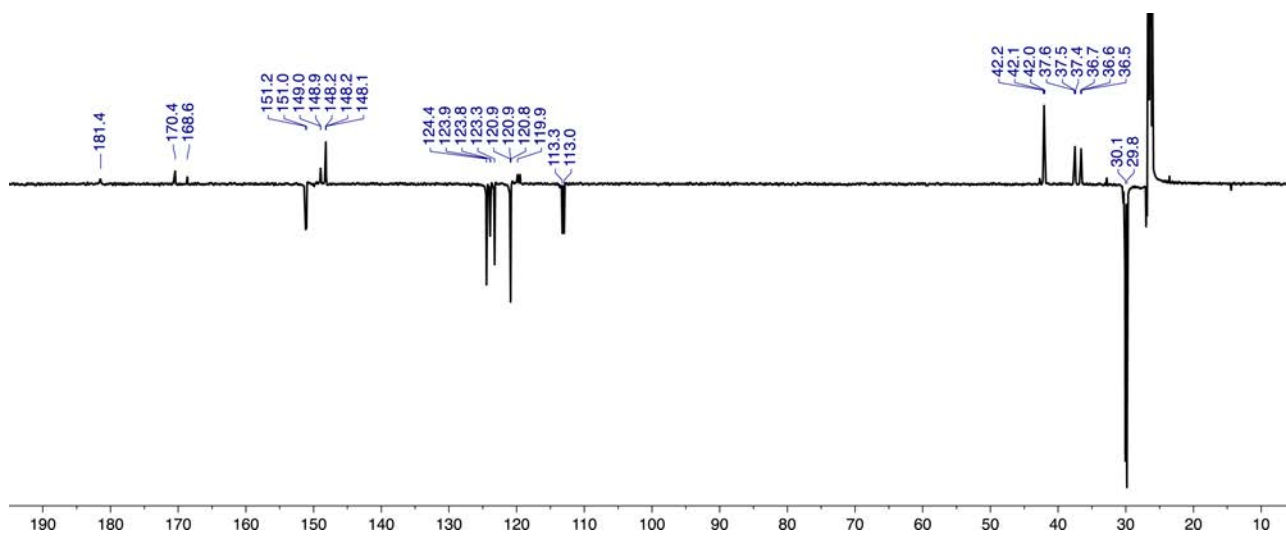


Figure S-15: $^{13}\text{C}\{^1\text{H}\}$ APT NMR spectrum of **3a** (C_6D_{12} , 126 MHz).

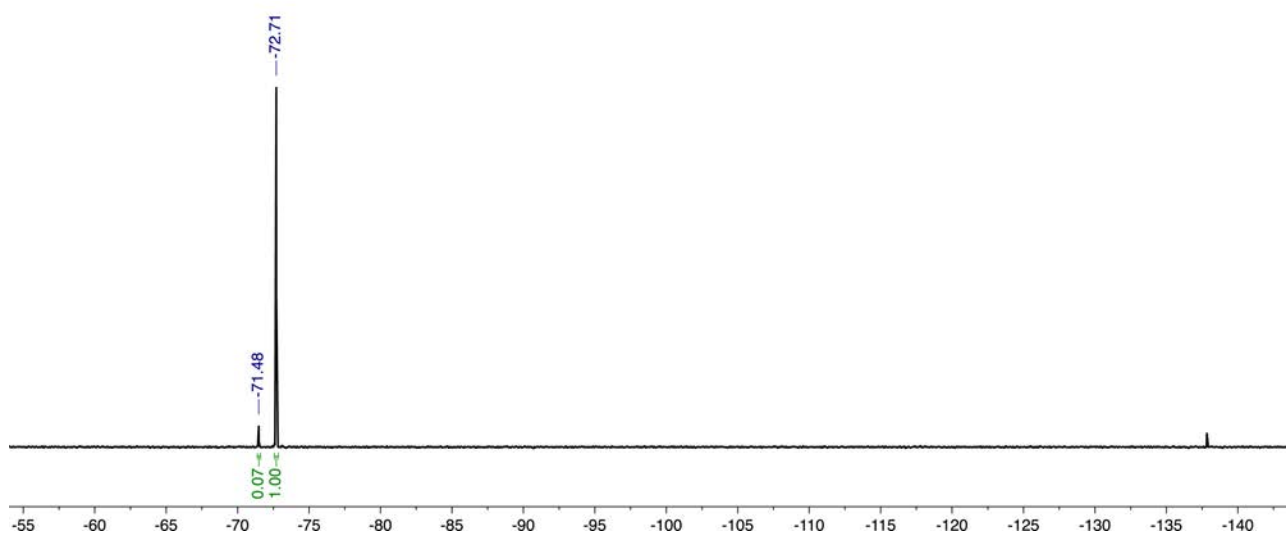


Figure S-16: $^{19}\text{F}\{^1\text{H}\}$ NMR spectrum of **3a** (C_6D_{12} , 377 MHz).

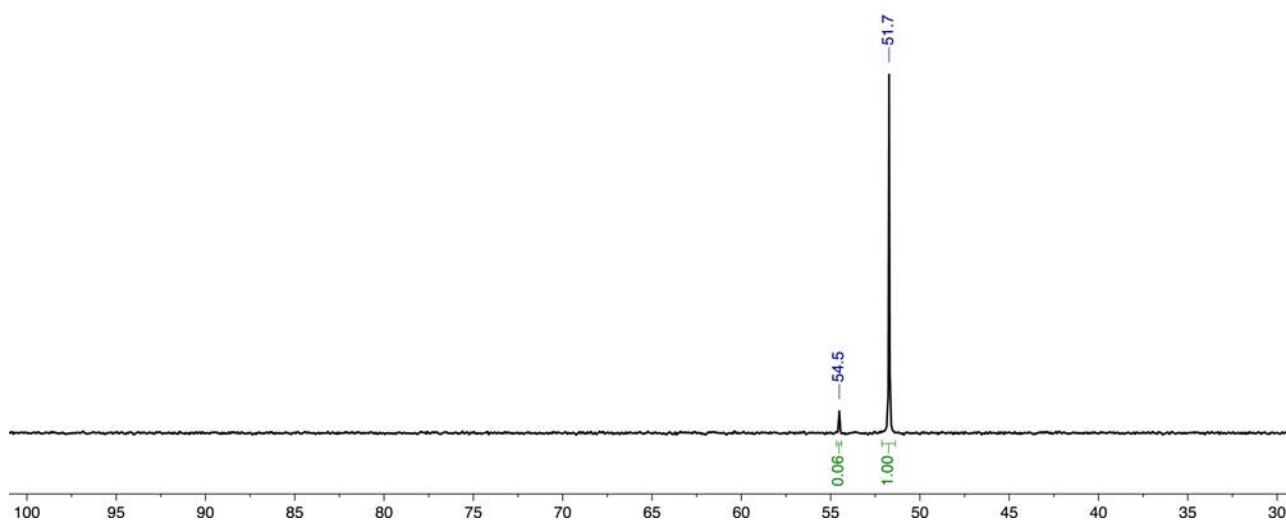


Figure S-17: $^{31}\text{P}\{^1\text{H}\}$ NMR spectrum of **3a** (C_6D_{12} , 202 MHz).

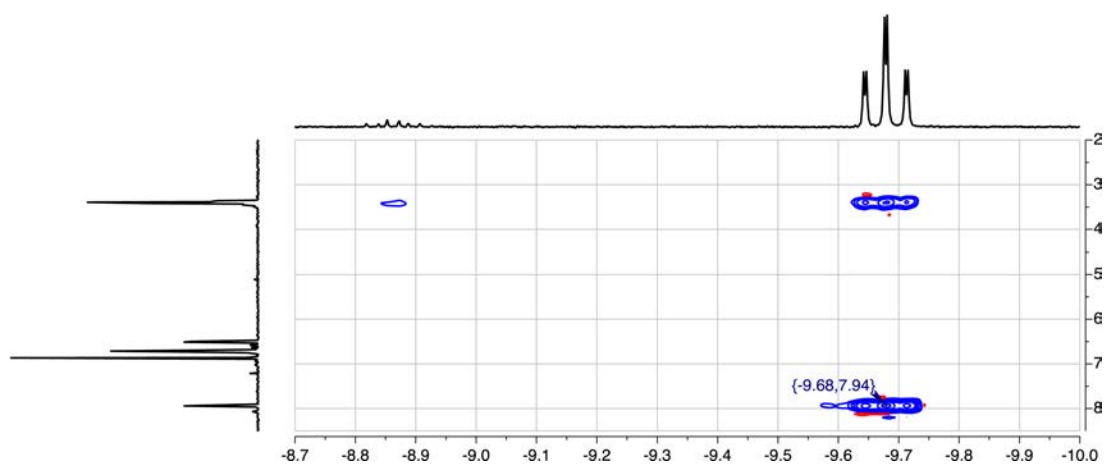


Figure S-18: NOESY spectrum (C_6D_{12} , 500 MHz).

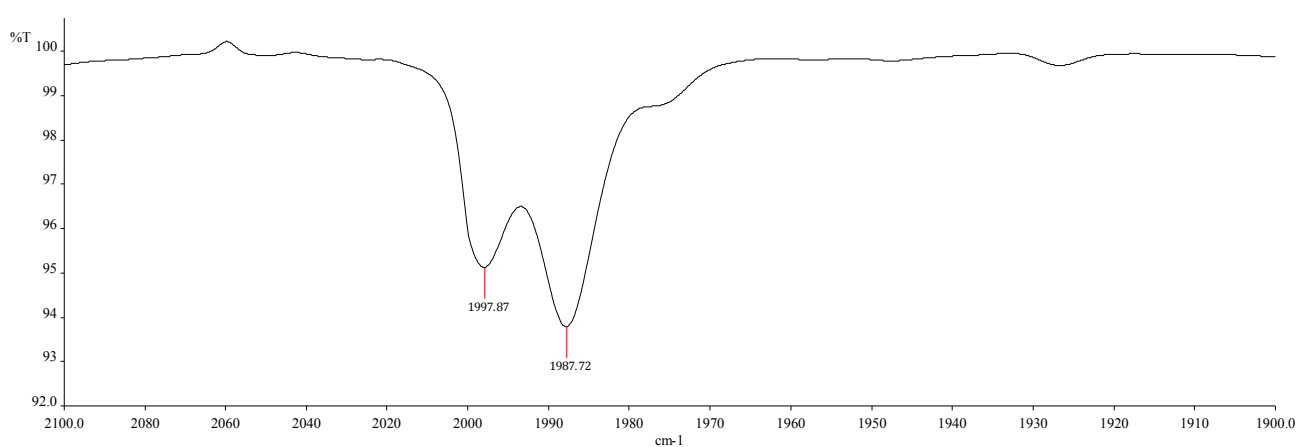


Figure S-19: Carbonyl stretching bands in the IR spectrum of **3a** (C_6H_{12}).

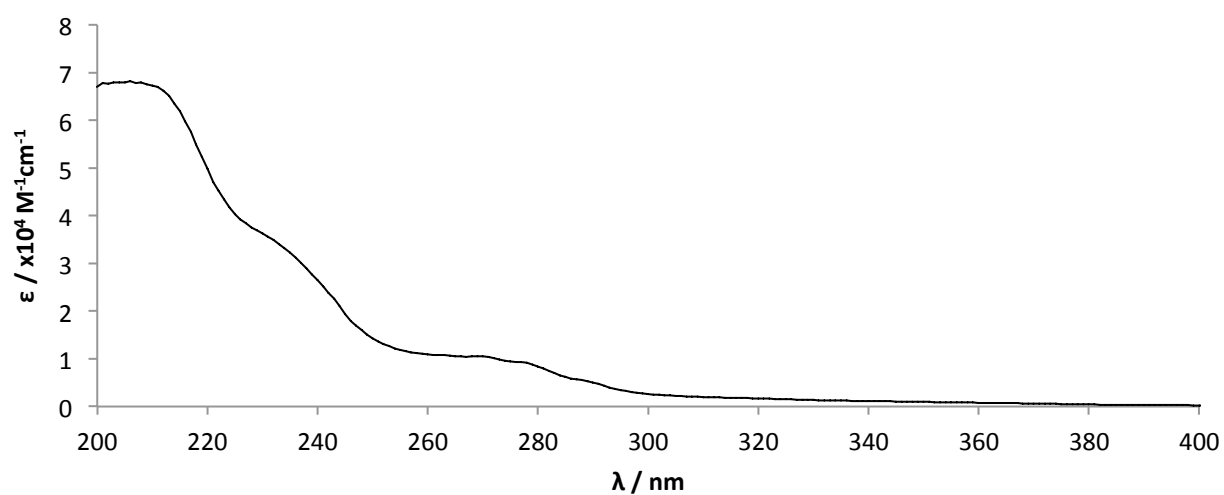


Figure S-20: UV-vis spectrum of **3a** (C_6H_{12}).

1.3.3 [Ir(2,6-($P^tBu_2CH_2$) $_2C_6H_3$)(2,3- $C_6H_3F_2$)H(CO)] (**3b**)

Prepared using the general procedure. Yield = 45%.

Single crystalline sample for analysis by X-ray diffraction grown from heptane at $-20\text{ }^\circ\text{C}$ (Figure 2).

Assignment of the rotamers was achieved by detection of an NOE interaction for Ir-H...H-Ar^F(C6) in the major rotamer (Figure S-25). This interaction is absent for the minor rotamer and instead ¹h_{J_{FH} coupling of 10.6 Hz for the Ir-H resonance is observed (cf. 10.8 for **3c**).}

¹H NMR (C₆D₁₂, 500 MHz, major rotamer): δ 7.62 – 7.66 (m, 1H, Ar^F), 6.88 (d, ³J_{HH} = 7.5, 2H, C₆H₃), 6.74 (t, ³J_{HH} = 7.5, 1H, C₆H₃), 6.41 – 6.53 (m, 2H, Ar^F), 3.43 (dt, ²J_{HH} = 16.2, J_{PH} = 4.2, 2H, CH₂), 3.39 (dt, ²J_{HH} = 16.2, J_{PH} = 3.4, 2H, CH₂), 1.19 (t, J_{PH} = 6.7, 18H, ^tBu), 1.17 (t, J_{PH} = 6.6, 18H, ^tBu), -9.66 (td, ³J_{PH} = 17.1, ⁴J_{FH} = 2.3, 1H, IrH). **¹H NMR** (C₆D₁₂, 500 MHz, selected data for minor rotamer): δ 7.74 – 7.78 (m, 1H, Ar^F), -8.88 (td, ³J_{PH} = 16.9, ¹h_{J_{FH}} = 10.6, 1H, IrH).

¹³C{¹H} NMR (C₆D₁₂, 126 MHz, major rotamer): δ 181.1 (m, CO), 169.5 (dd, ¹J_{FC} = 226, ²J_{FC} = 9, Ar^F), 150.8 (dd, ¹J_{FC} = 251, ²J_{FC} = 24, Ar^F), 148.1 (t, J_{PC} = 6, C₆H₃{CCH₂}), 144.9 (dd, ³J_{FC} = 16, ⁴J_{FC} = 4, Ar^F), 124.6 (s, C₆H₃), 124.2 (dm, ²J_{FC} = 41, Ar^F{IrC}), 123.1 (br, Ar^F), 121.0 (t, J_{PC} = 7, C₆H₃), 110.8 (d, ²J_{FC} = 18, Ar^F), 41.9 (t, J_{PC} = 15, CH₂), 37.5 (t, J_{PC} = 13, ^tBu{C}), 36.6 (t, J_{PC} = 10, ^tBu{C}), 30.1 (s, ^tBu{Me}), 29.8 (s, ^tBu{Me}). The C₆H₃{IrC} resonance could not be unambiguously assigned.

¹⁹F{¹H} NMR (C₆D₁₂, 377 MHz): δ -98.25 (d, ³J_{FF} = 28.5, 1F / minor rotamer), -99.13 (d, ³J_{FF} = 28.6, 1F / major rotamer), -139.07 (d, ³J_{FF} = 28.6, 1F / major rotamer), -139.52 (d, ³J_{FF} = 28.5, 1F / minor rotamer).

³¹P{¹H} NMR (C₆D₁₂, 202 MHz): δ 54.7 (s, minor rotamer), 52.2 (s, major rotamer). **³¹P{¹H} NMR** (1,2-C₆H₄F₂/C₆D₆, 202 MHz): δ 52.1 (s, major rotamer).

Anal. Calcd. for C₃₁H₄₇F₂IrOP₂ (727.88 g·mol⁻¹): C, 51.15; H, 6.51; N, 0.00. Found: C, 51.03; H, 6.61; N, 0.00.

IR (C₆H₁₂): ν(CO) = 1989.9, 2000.1 cm⁻¹.

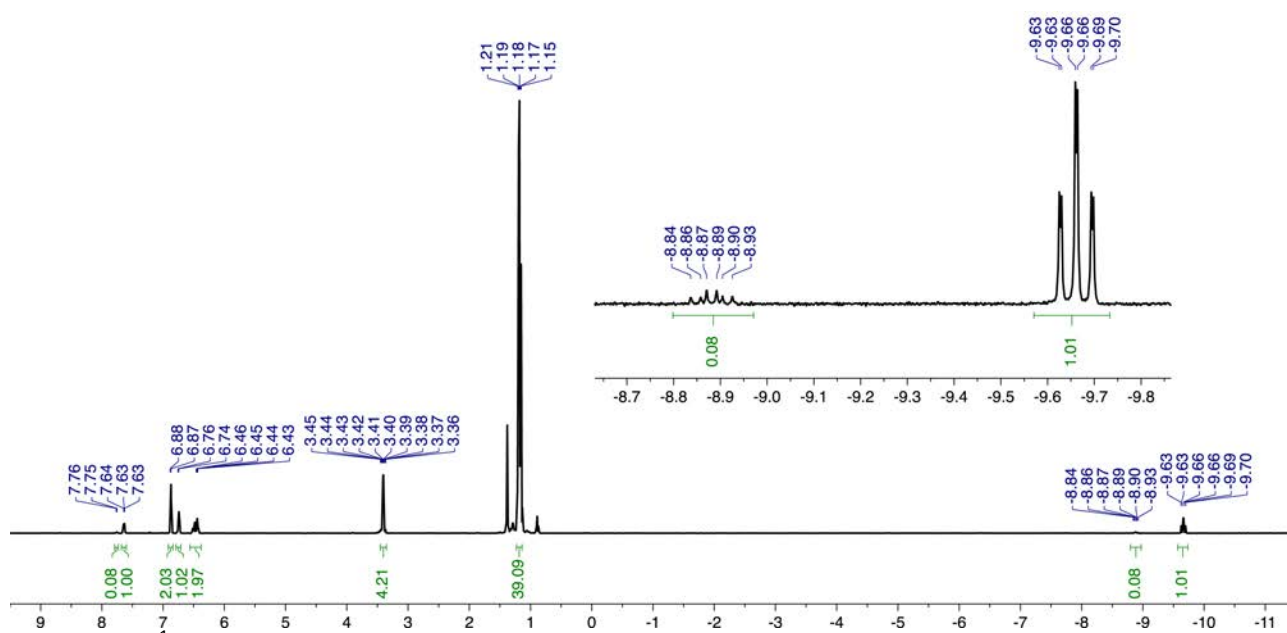


Figure S-21: ¹H NMR spectrum of **3b** (C₆D₁₂, 500 MHz).

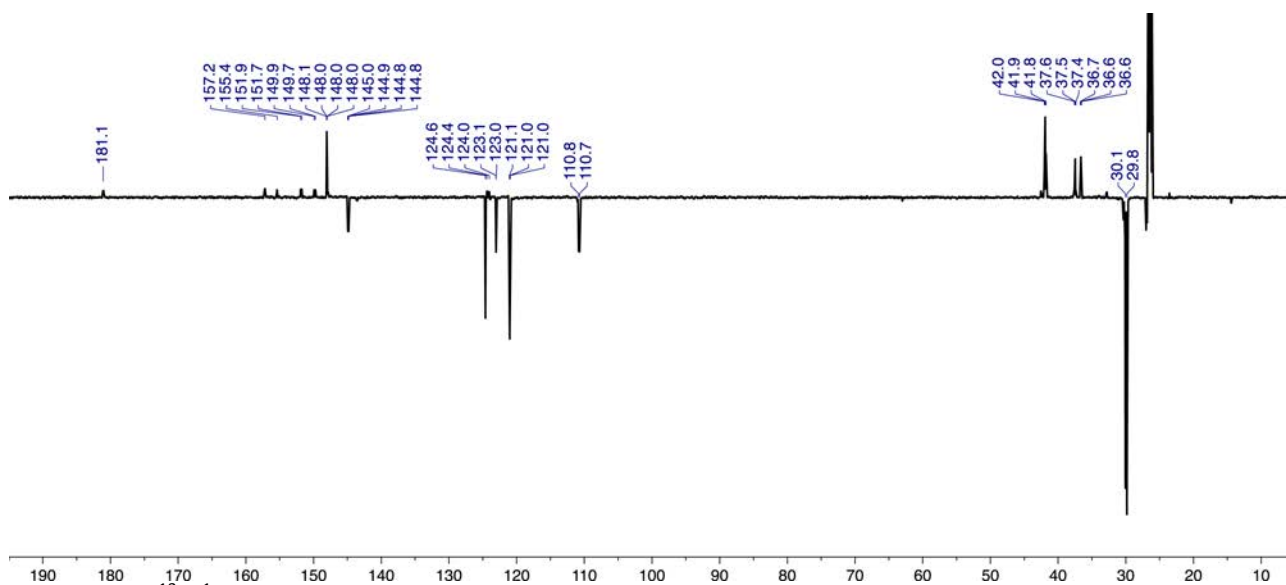


Figure S-22: $^{13}\text{C}\{^1\text{H}\}$ APT NMR spectrum of **3b** (C_6D_{12} , 126 MHz).

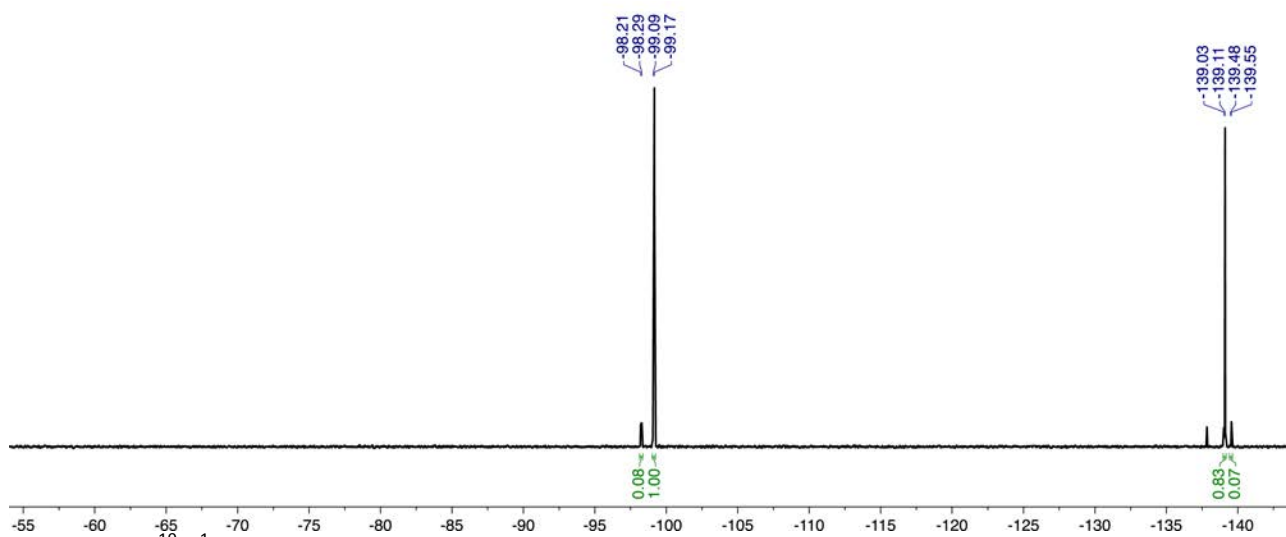


Figure S-23: $^{19}\text{F}\{^1\text{H}\}$ NMR spectrum of **3b** (C_6D_{12} , 377 MHz).

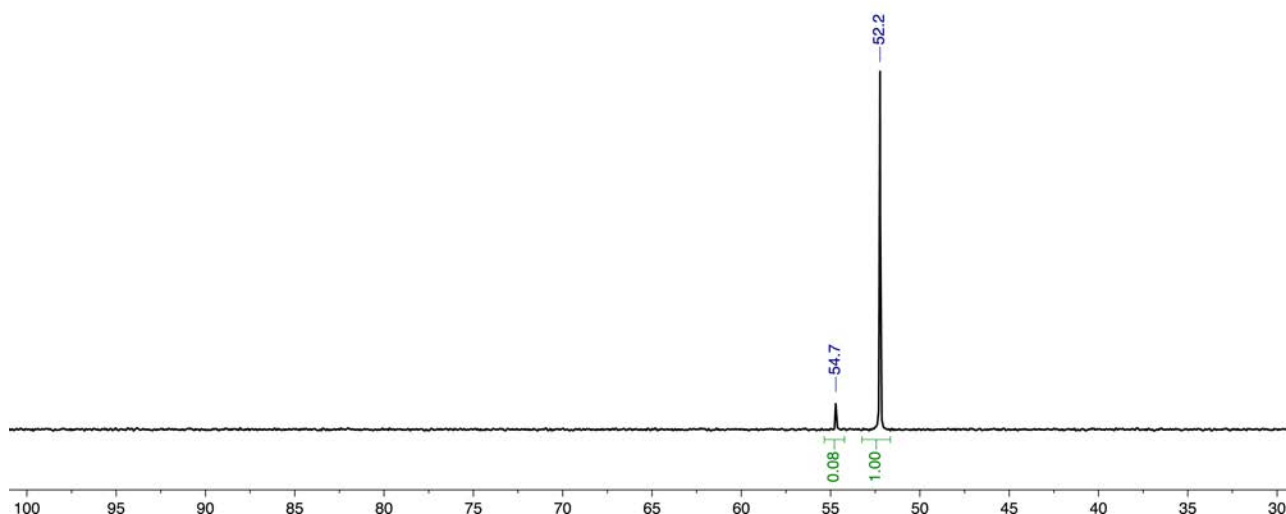


Figure S-24: $^{31}\text{P}\{^1\text{H}\}$ NMR spectrum of **3b** (C_6D_{12} , 202 MHz).

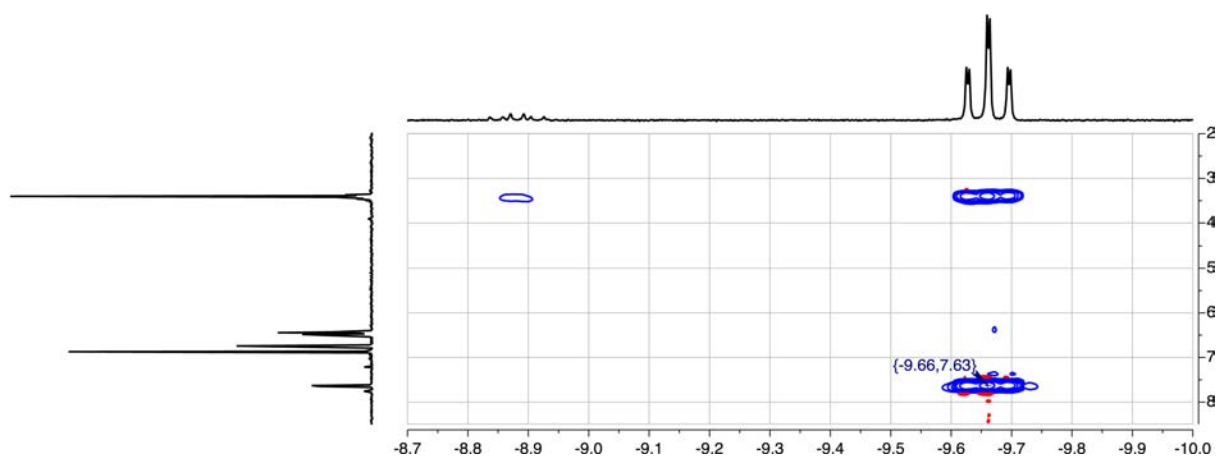


Figure S-25: NOESY spectrum (C_6D_{12} , 500 MHz).

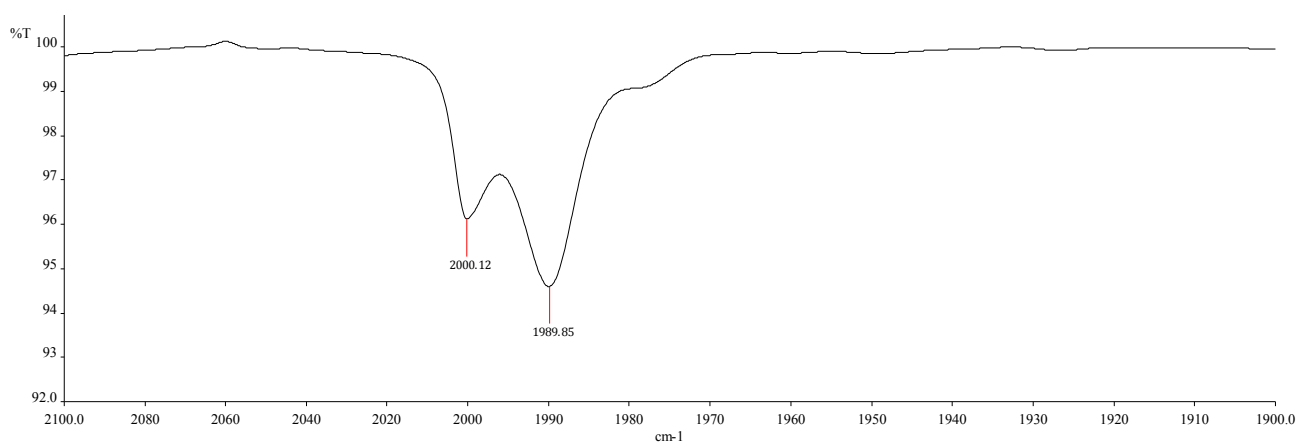


Figure S-26: Carbonyl stretching bands in the IR spectrum of **3b** (C_6H_{12}).

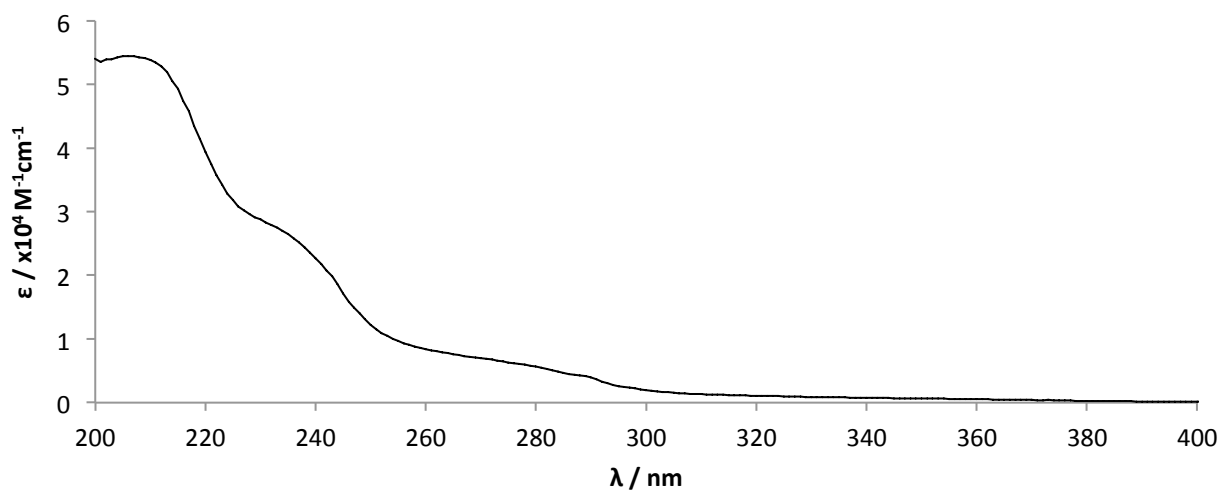


Figure S-27: UV-vis spectrum of **3b** (C_6H_{12})

1.3.4 [Ir(2,6-(P^tBu₂CH₂)₂C₆H₃)(2,4,6-C₆H₂F₃)H(CO)] (3c)

Prepared using the general procedure. Yield = 49%.

Single crystalline sample for analysis by X-ray diffraction grown from heptane at -20 °C (Figure S-37).

¹H NMR (C₆D₁₂, 500 MHz): δ 6.88 (d, ³J_{HH} = 7.5, 2H, C₆H₃), 6.76 (t, ³J_{HH} = 7.5, 1H, C₆H₃), 6.39 (tt, ³J_{FH} = 8.3, ⁴J_{FH} = 1.8, 2H, Ar^F), 6.32 (tt, ³J_{FH} = 8.6, ⁴J_{FH} = 2.1, 2H, Ar^F), 3.42 (br t, J_{PH} = 3.5, 4H, CH₂), 1.19 (t, J_{PH} = 6.6, 18H, ^tBu), 1.14 (t, J_{PH} = 6.7, 18H, ^tBu), -9.46 (tdd, ³J_{PH} = 16.7, ^{1h}J_{FH} = 10.8, J = 2.9, 1H, IrH).

¹³C{¹H} NMR (C₆D₁₂, 126 MHz): δ 180.9 (m, CO), 169.2 (ddd, ¹J_{FC} = 228, ³J_{FC} = 26, ³J_{FC} = 14, Ar^F), 168.8 (ddd, ¹J_{FC} = 231, ³J_{FC} = 25, ³J_{FC} = 13, Ar^F), 162.3 (dt, ¹J_{FC} = 241, ³J_{FC} = 17, Ar^F), 147.7 (t, J_{PC} = 6, C₆H₃{CCH₂}), 147.0 (t, J_{PC} = 4, C₆H₃{IrC}), 124.7 (s, C₆H₃), 121.3 (t, J_{PC} = 7, C₆H₃), 101.1 (t, J_{FC} = 52, Ar^F{IrC}), 98.0 (ddd, ²J_{FC} = 40, ²J_{FC} = 23, ⁴J_{FC} = 4, Ar^F), 97.6 (ddd, ²J_{FC} = 41, ²J_{FC} = 23, ⁴J_{FC} = 4, Ar^F), 41.9 (t, J_{PC} = 15, CH₂), 37.0 (t, J_{PC} = 9, ^tBu{C}), 36.2 (t, J_{PC} = 13, ^tBu{C}), 30.4 (s, ^tBu{Me}), 30.0 (s, ^tBu{Me}).

¹⁹F{¹H} NMR (C₆D₁₂, 377 MHz): δ -64.49 (d, ⁴J_{FF} = 7.0, 1F), -65.41 (d, ⁴J_{FF} = 7.0, 1F), -120.98 (t, ⁴J_{FF} = 7.0).

³¹P{¹H} NMR (C₆D₁₂, 202 MHz): δ 54.0 (s). ³¹P{¹H} NMR (1,3,5-C₆H₃F₃/C₆D₆, 202 MHz): δ 53.7 (s).

Anal. Calcd. for C₃₁H₄₆F₃IrOP₂ (745.87 g·mol⁻¹): C, 49.92; H, 6.22; N, 0.00. Found: C, 50.04; H, 6.27; N, 0.00.

IR (C₆H₁₂): ν(CO) = 1992.5, 2002.2 cm⁻¹.

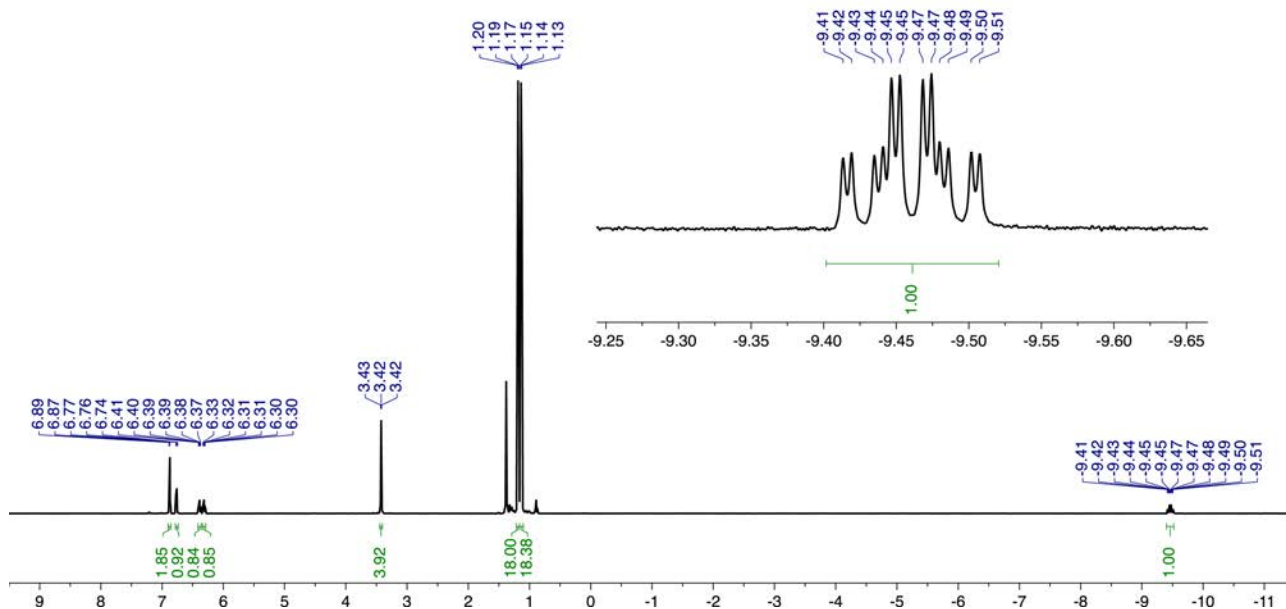


Figure S-28: ¹H NMR spectrum of 3c (C₆D₁₂, 500 MHz).

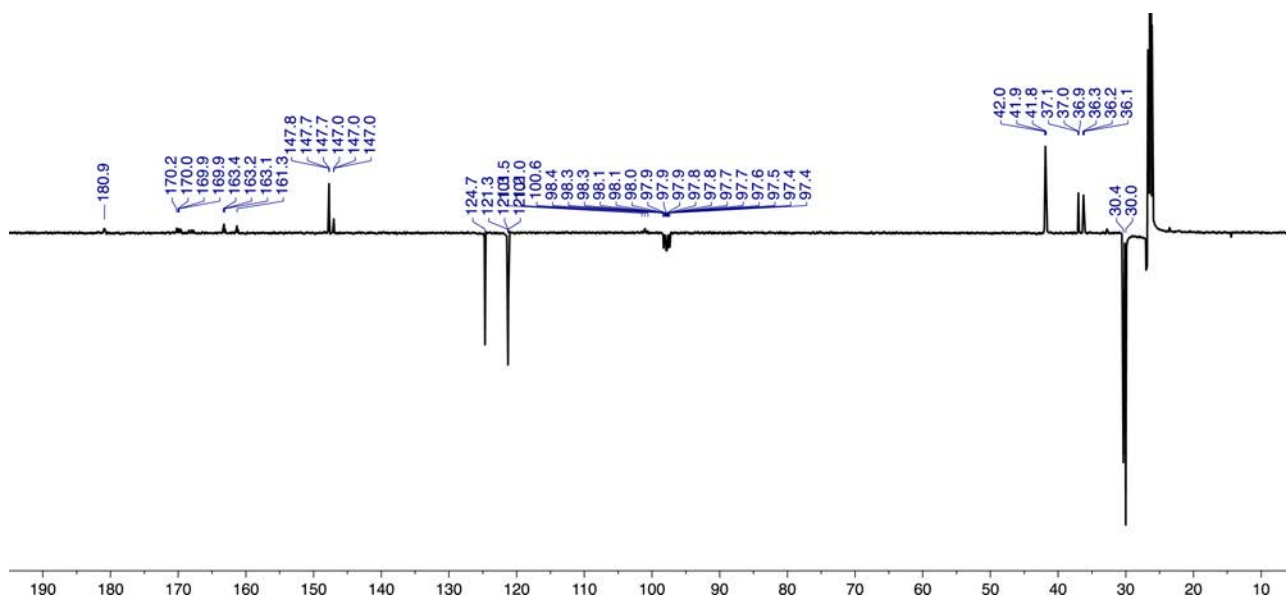


Figure S-29: $^{13}\text{C}\{^1\text{H}\}$ APT NMR spectrum of **3c** (C_6D_{12} , 126 MHz).

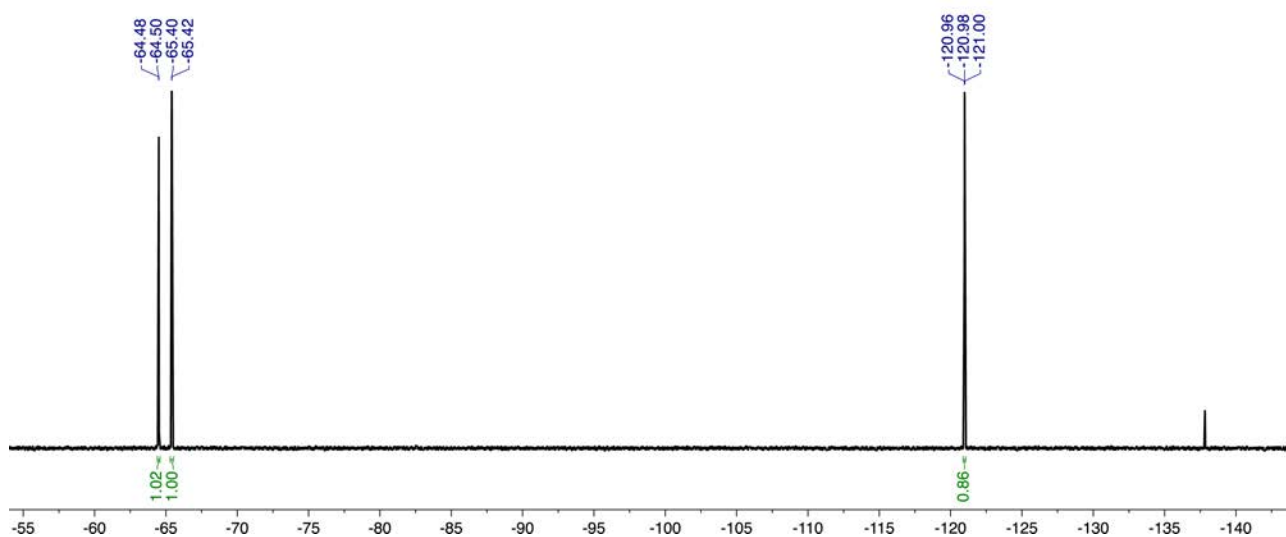


Figure S-30: $^{19}\text{F}\{^1\text{H}\}$ NMR spectrum of **3c** (C_6D_{12} , 377 MHz).

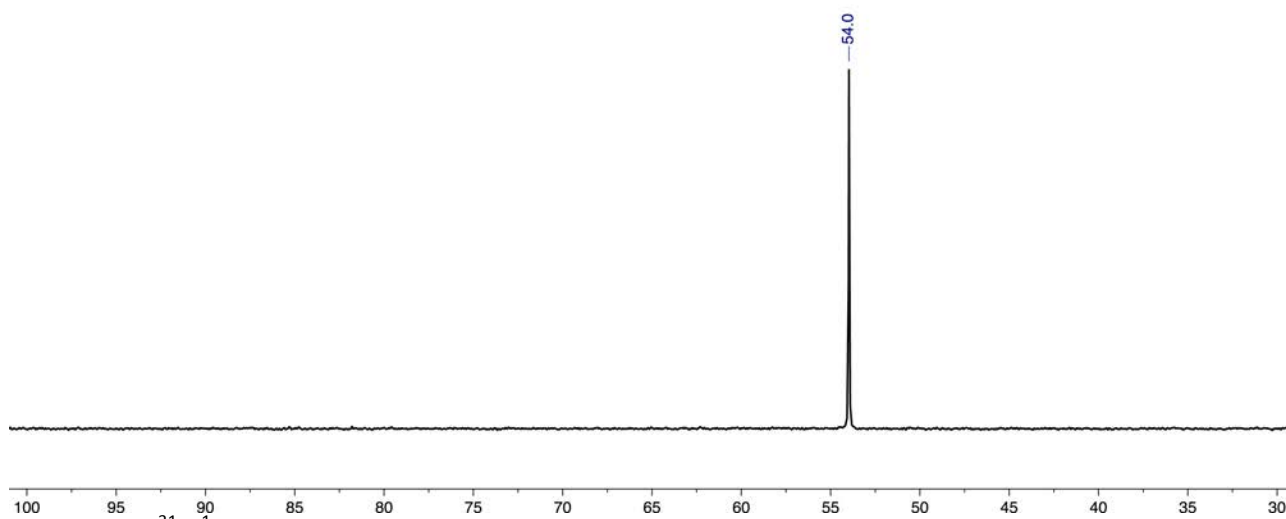


Figure S-31: $^{31}\text{P}\{^1\text{H}\}$ NMR spectrum of **3c** (C_6D_{12} , 202 MHz).

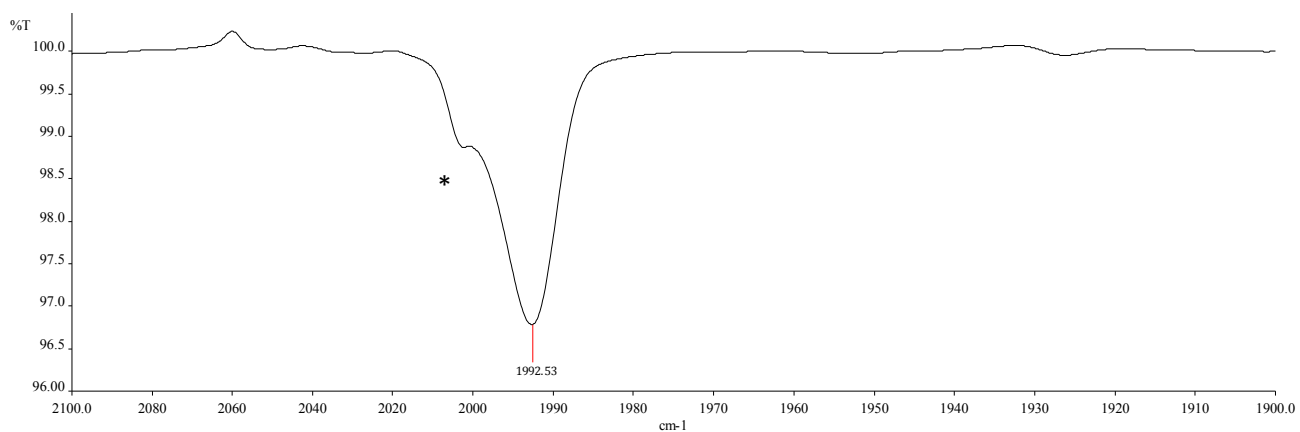


Figure S-32: Carbonyl stretching bands in the IR spectrum of **3c** (C₆H₁₂). * Shoulder = 2002.23 cm⁻¹.

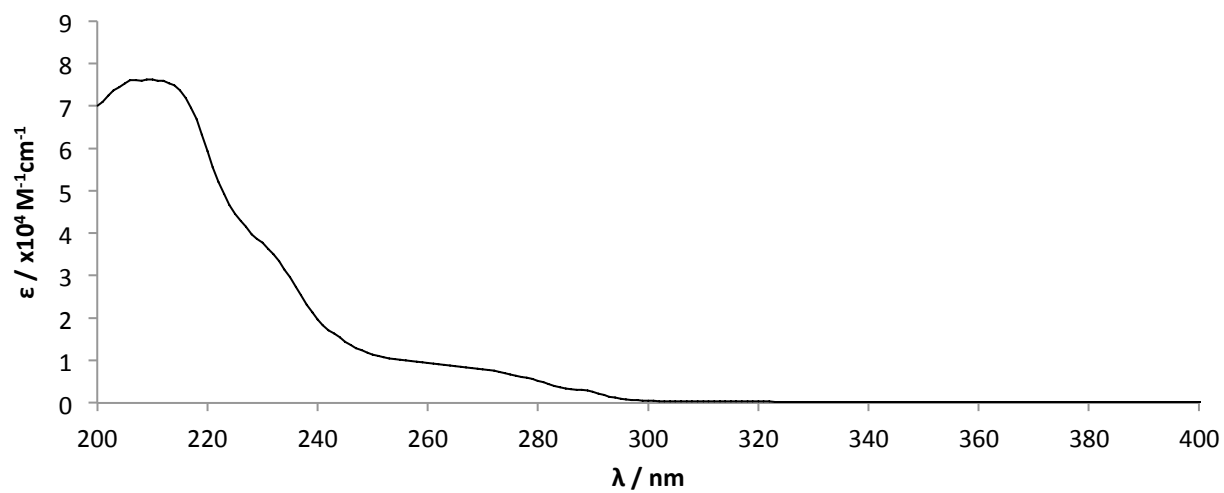


Figure S-33: UV-vis spectrum of **3c** (C₆H₁₂)

1.4 Crystallography

Full crystallographic details including solution, refinement and disorder modelling procedures are documented in CIF format and have been deposited with the Cambridge Crystallographic Data Centre under CCDC 1520522 (**2**), 1520523 (**3a**), 1520524 (**3b**), 1520525 (**3c**). These data can be obtained free of charge from The Cambridge Crystallographic Data Centre via www.ccdc.cam.ac.uk/data_request/cif.

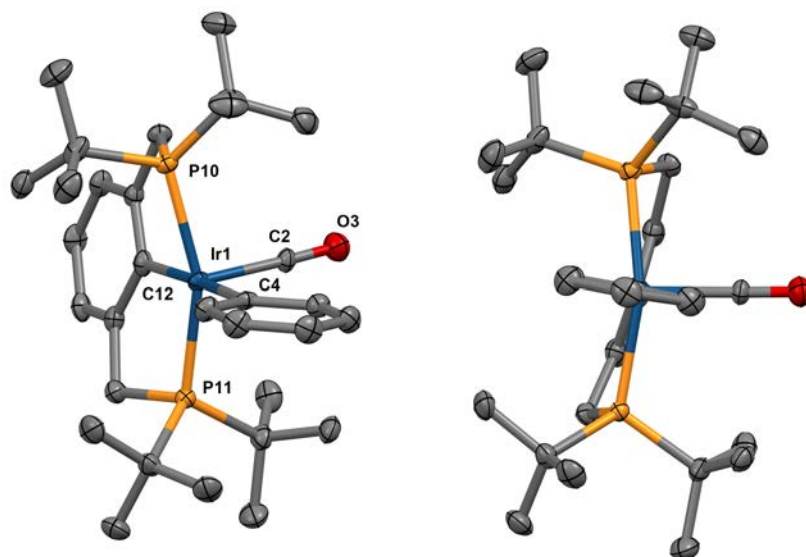


Figure S-34: Solid-state structure of **2** (left, with numbering; right, viewed along the Ir1-C12 vector). Thermal ellipsoids at 50% probability level; hydrogen atoms omitted for clarity. Selected bond lengths [Å] and angles [°]: Ir1-C2, 1.923(4); Ir1-C4, 2.156(4); Ir1-C12, 2.119(4); Ir1-P10, 2.3344(11); Ir1-P11, 2.3394(11); C2-Ir1-C12, 91.15(17); C4-Ir1-C12, 174.61(17); P10-Ir1-P11, 157.21(4).

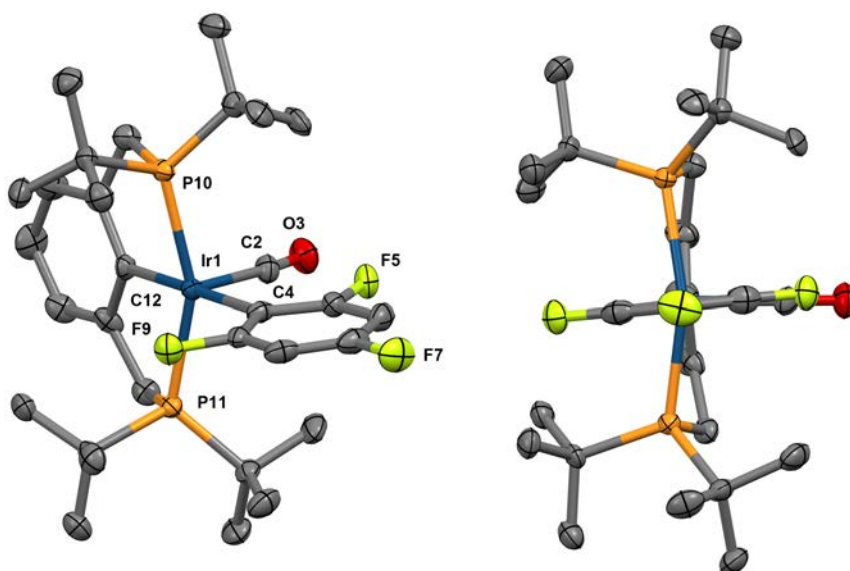


Figure S-35: Solid-state structure of **3c** (left, with numbering; right, viewed along the Ir1-C12 vector). Thermal ellipsoids at 50% probability level; hydrogen atoms omitted for clarity. Selected bond lengths [Å] and angles [°]: Ir1-C2, 1.944(5); Ir1-C4, 2.178(5); Ir1-C12, 2.113(4); Ir1-P10, 2.3569(12); Ir1-P11, 2.3520(12); C2-Ir1-C12, 83.1(2); C4-Ir1-C12, 179.75(18); P10-Ir1-P11, 156.54(4).

2 Computational details

2.1 Geometry optimisations and free energy calculations

Density functional theory (DFT) calculations were implemented in the Gaussian 03 suite of programs.⁶ Based on successful implementation in related systems,⁷ calculations were carried out at the BP86 level in combination with the LANL2DZ effective core potential (ECP) and basis set for iridium, and 6-31G** basis sets were for all other atoms.⁸

Geometry optimisations were performed without symmetry constraints based on starting geometries prepared in the following ways:

- The major rotamers of **1**, **2** and **3a-c** were initiated from the respective crystal structures. The hydride ligands were added manually.
- Isomers of **3a-b** are based on transposed optimised structures of **3a-b**.
- Carbonyl dissociated intermediates **1'**, **2'** and **3a'-c'** (see Figure S-36, S-37) were constructed by deletion of CO atoms from the corresponding optimised structure. Several starting geometries of the 5-coordinate intermediate **2'** were considered, but all optimised to the same square pyramidal geometry.
- CO, benzene, fluorobenzene, 1,2-difluorobenzene and 1,3,5-trifluorobenzene were optimised from handmade structures.

Optimised geometries provided in xyz format.

Normal mode analyses verified the located stationary points as minima on the potential energy surface. Thermal corrections (298.15 K, 1 atm) were applied to deduce the Gibbs free energies of all optimised species. Summation of these energies without further correction allows construction of an approximate reaction pathway (Figure S-37), although transition states and σ -CH intermediates have not been considered. The calculated Gibbs free energies of the various isomers of **3a-b** and **3a'-b'** are shown in Figure S-36 and predict in each instance the correct lowest energy isomer (*syn* to carbonyl, *ortho* to iridium).

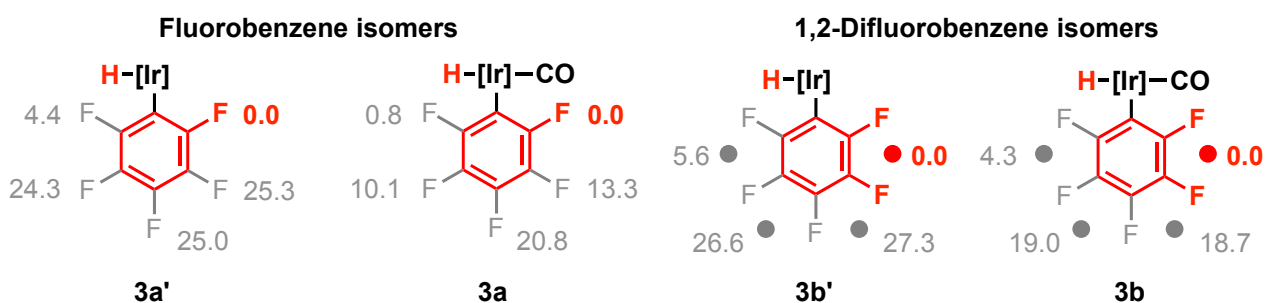


Figure S-36: Calculated Gibbs free energies of the regioisomers and rotamers of **3a**, **3b**, **3a'** and **3b'** expressed in kJ·mol⁻¹ relative to the lowest energy isomer. Experimentally observed major isomer in bold.

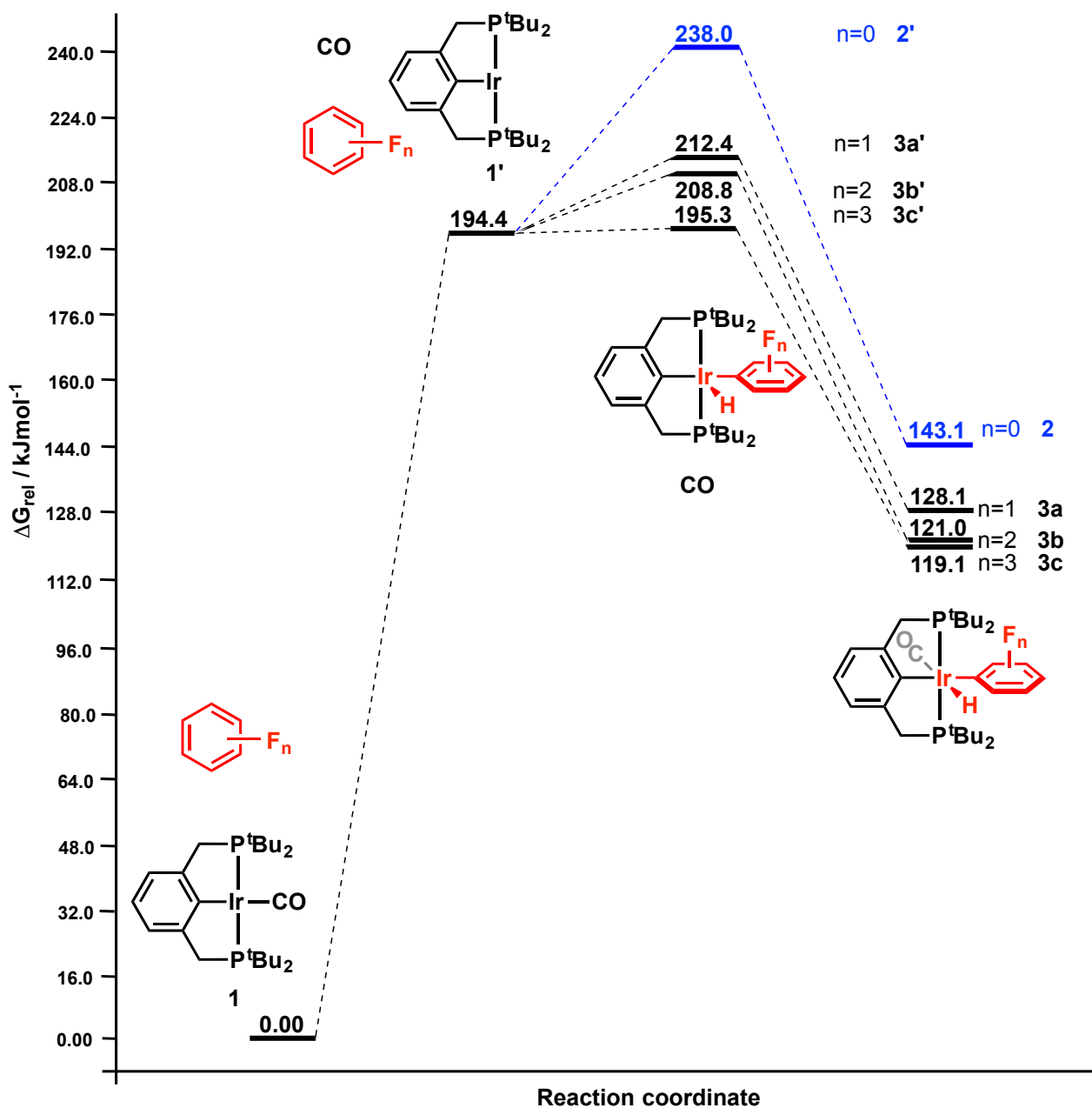


Figure S-37: Calculated Gibbs free energy pathway (based on key intermediates) for the C–H bond activation of benzene, fluorobenzene, 1,2-difluorobenzene and 1,3,5-trifluorobenzene (298 K).

Table S-1: Calculated thermodynamic parameters for key intermediates in the C–H bond activation of benzene, fluorobenzene, 1,2-difluorobenzene and 1,3,5-trifluorobenzene (298 K). $E_0 = E_{elec} + ZPE$; $E = E_0 + E_{vib} + E_{rot} + E_{trans}$; $H = E + RT$; $G = H - TS$

Relative energies of benzene activation /kJ·mol ⁻¹				
	1 + C₆H₆	1' + CO + C₆H₆	2' + CO	2
<i>E</i>₀	0.00	240.5	225.0	80.5
<i>E</i>	0.00	242.0	229.2	82.3
<i>H</i>	0.00	244.5	229.2	79.8
<i>G</i>	0.00	194.4	238.0	143.1

Relative energies of fluorobenzene activation /kJ·mol ⁻¹				
	1 + C₆H₅F	1' + CO + C₆H₅F	3a' + CO	3a
<i>E</i>₀	0.00	240.5	197.3	63.1
<i>E</i>	0.00	242.0	201.1	64.3
<i>H</i>	0.00	244.5	201.1	61.8
<i>G</i>	0.00	194.4	212.4	128.1

Relative energies of 1,2-difluorobenzene activation /kJ·mol ⁻¹				
	1 + C₆H₄F₂	1' + CO + C₆H₄F₂	3b' + CO	3b
<i>E</i>₀	0.00	240.5	192.5	57.5
<i>E</i>	0.00	242.0	196.1	59.3
<i>H</i>	0.00	244.5	196.1	56.8
<i>G</i>	0.00	194.4	208.8	121.0

Relative energies of 1,3,5-trifluorobenzene /kJ·mol ⁻¹				
	1 + C₆H₃F₃	1' + CO + C₆H₃F₃	3c' + CO	3c
<i>E</i>₀	0.00	240.5	176.2	52.0
<i>E</i>	0.00	242.0	179.4	53.4
<i>H</i>	0.00	244.5	179.4	50.9
<i>G</i>	0.00	194.4	195.3	119.1

2.2 Infrared vibrational modes

The normal mode analysis of **2**, **3a-c** predicts the coupling of the carbonyl stretching modes to the *trans* hydride (Figure S-38), resulting in two carbonyl stretching modes as observed experimentally (*vide supra*).

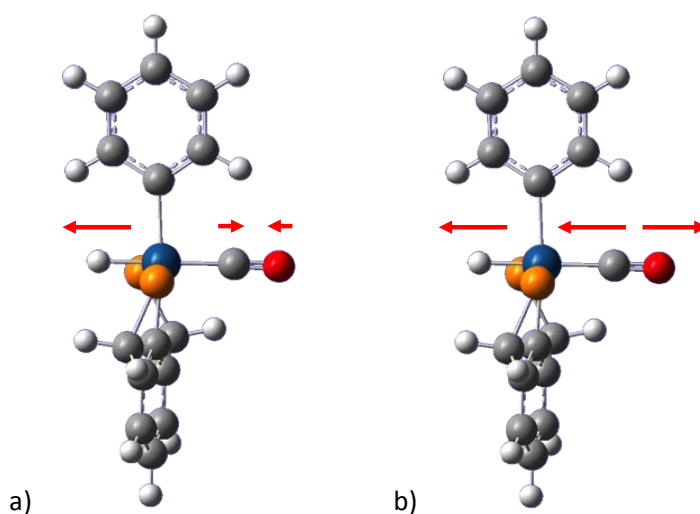


Figure S-38: Graphical representation of the (a) symmetric and (b) antisymmetric carbonyl stretching modes of **2** (^tBu groups omitted for clarity). Arrows represent the approximate magnitude of atom displacement.

Table S-2: Calculated and experimental carbonyl stretching frequencies for **1** – **3**.

Complex	Mode	Frequency /cm ⁻¹	
		Exp.	Calcd.
1	-	1926.8	1933.6
2	antisymmetric	1981.7	1938.8
	symmetric	1971.1	2092.6
3a	antisymmetric	1987.7	1953.7
	symmetric	1997.9	2102.8
3b	antisymmetric	1989.9	1951.8
	symmetric	2000.1	2091.0
3c	antisymmetric	1992.5	1958.3
	symmetric	2002.2	2122.6

2.3 TD-DFT calculations and assignment of UV-vis spectra

2.3.1 Methodology

Time-dependant DFT (TD-DFT) calculations for **1** and **2** were carried out using the Orca 3.0.3 suite of programs.⁹ After assessing several density functional and basis set combinations, the greatest correspondence to the experimentally derived UV-Vis spectra was achieved using the double-hybrid B2PLYP functional (53% HF exchange, 27% MP2 correlation) in combination with the DEF2-SD ECP and DEF2-TZVP basis set and auxiliary basis for iridium, and 6-31G** basis sets with an SD auxiliary set for all other atoms.¹⁰ The RIJCOSX algorithm was employed throughout.¹¹ The first 40 singlet-singlet excitations and their associated natural transition orbitals (NTOs) were assessed, with major (>10% contribution) constituent NTOs for all transitions with an oscillator strength greater than 0.01 qualitatively assigned. NTO surface plots were constructed with Orca and rendered in GaussView 5.0. Transitions of interest, associated with a weakening of the M-CO bond were then identified as excitations which populate M-CO π^* and M-CO σ^* antibonding orbitals or depopulate M-CO π and M-CO σ bonding orbitals.

2.3.2 TD-DFT analysis of **1**

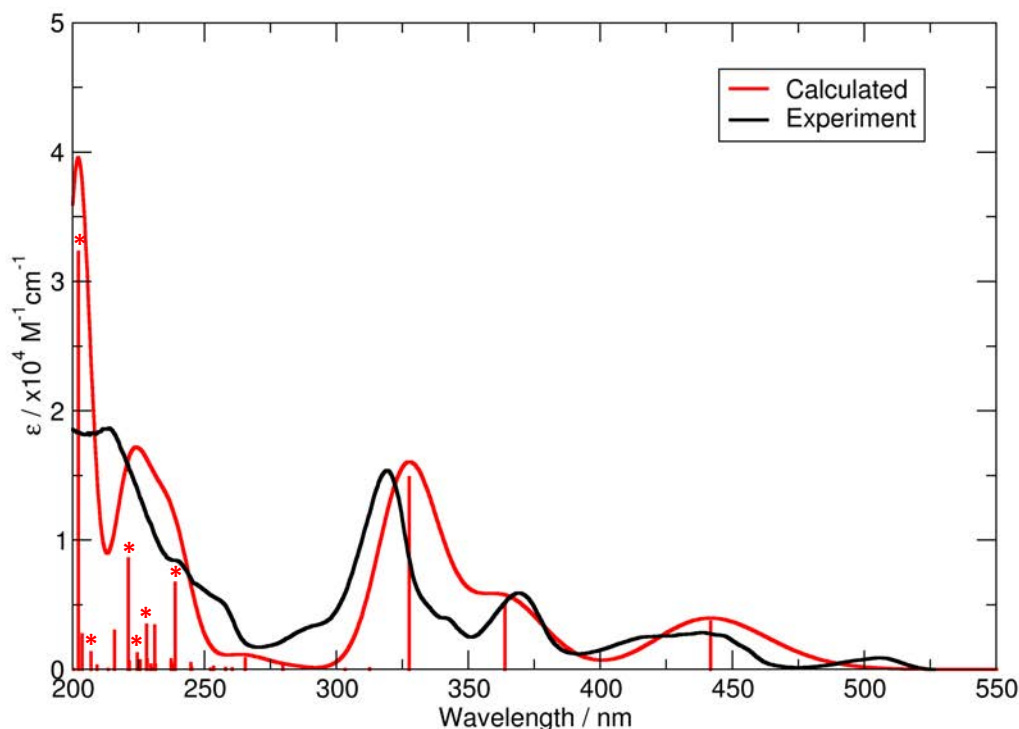
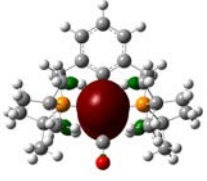
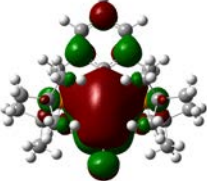
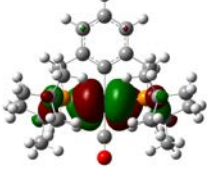
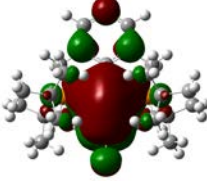
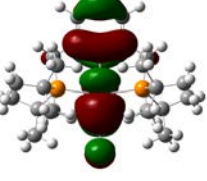
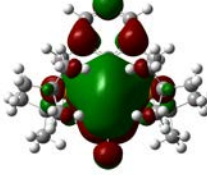
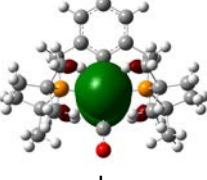
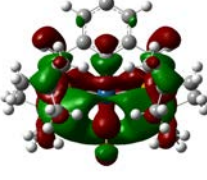
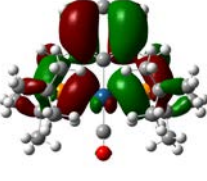
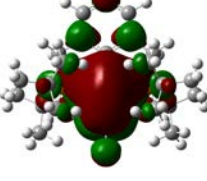
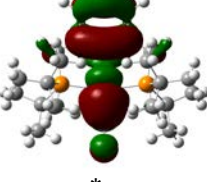
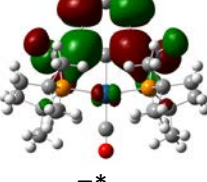
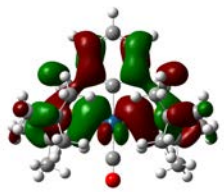
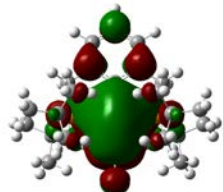
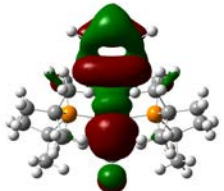
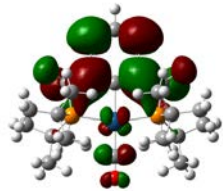
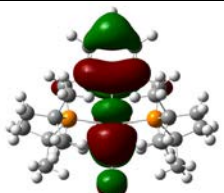
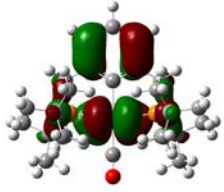
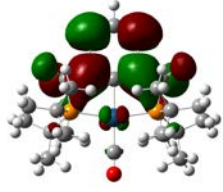
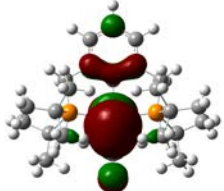
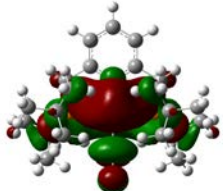
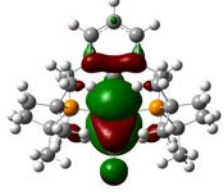
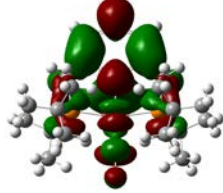
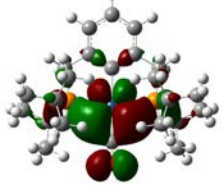
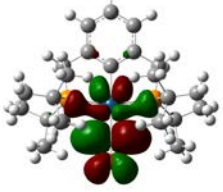
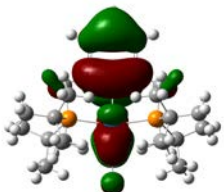
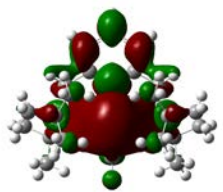
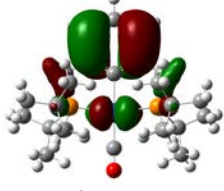
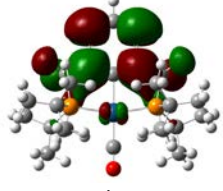
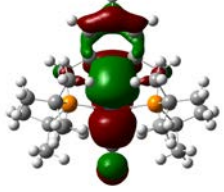
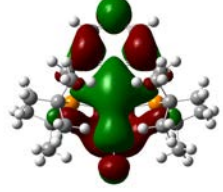
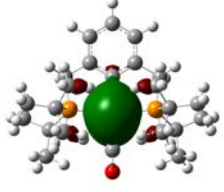
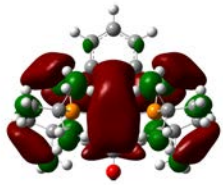
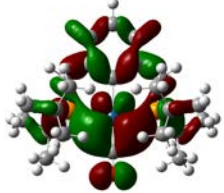
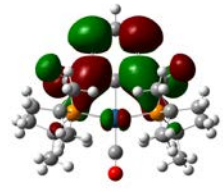
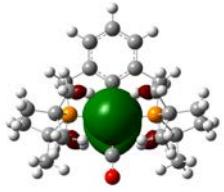
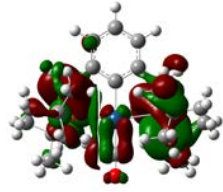
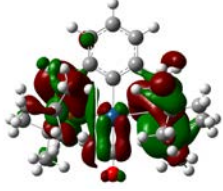
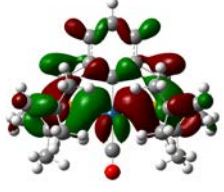
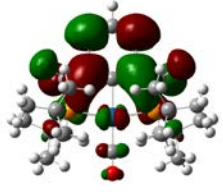


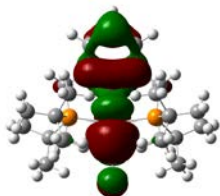
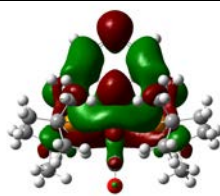
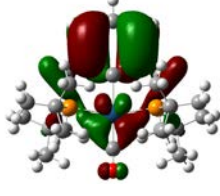
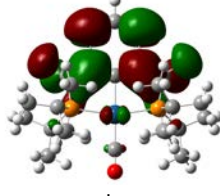
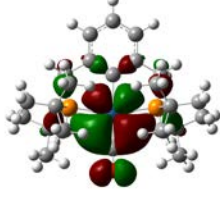
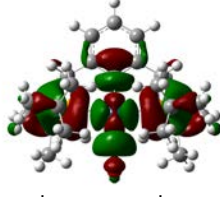
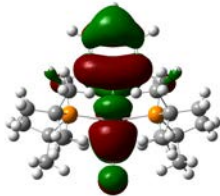
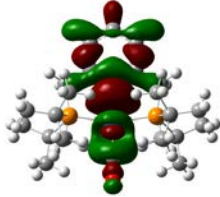
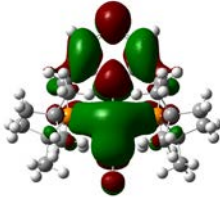
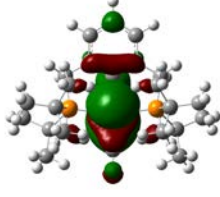
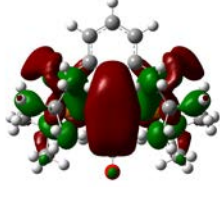
Figure S-39: Overlay of experimental and calculated UV-vis spectra of **1**. Gaussian convolution applied to calculated vertical transitions with a FWHM of 6700 cm^{-1} . Vertical transitions depicted at an arbitrary relative intensity for graphical clarity. Excitations marked with asterisks correspond to $\pi_{\text{M-CO}} \rightarrow \pi^*_{\text{M-CO}}$ or $\pi_{\text{M-CO}} \rightarrow \text{non-bonding}_{\text{M-CO}}$ transitions.

Table S-3: TD-DFT derived excitation energies for **1** restricted to those with oscillator strengths (f) greater than 0.01. Calculated NTOs with a greater than 10% contribution to a given excitation are shown rendered with an isosurface value of 0.02 and the major constituent molecular and atomic orbitals assigned.

State	λ / nm	f	Contributing Natural Transition Orbitals		
1	441.8	0.0463	 d_{z^2}	 $\pi_{\text{aryl-Ir-CO}}; \pi^*_{\text{aryl}}$	99%
3	363.8	0.0638	 d_{yz}	 $\pi_{\text{aryl-Ir-CO}}; \pi^*_{\text{aryl}}$	98%
2	327.5	0.1855	 $\pi_{\text{Ir-CO}}; \pi^*_{\text{Ir-aryl}}; \pi_{\text{aryl}}$	 $\pi_{\text{aryl-Ir-CO}}; \pi^*_{\text{aryl}}$	92%
18	265.4	0.0105	 d_{z^2}	 P centred	98%
15	238.9	0.0837	 $p_p; \pi_{\text{aryl}}$	 $\pi_{\text{aryl-Ir-CO}}; \pi^*_{\text{aryl}}$	54%
			 $\pi_{\text{Ir-CO}}; \pi^*_{\text{Ir-aryl}}; \pi_{\text{aryl}}$	 π^*_{aryl}	41%

17	231.1	0.0421	 $p_P; \pi_{\text{aryl}}$	→	 $\pi_{\text{aryl-Ir-CO}}; \pi^*_{\text{aryl}}$	78%
			 $\pi_{\text{Ir-CO}}; \pi^*_{\text{Ir-aryl}}; \pi_{\text{aryl}}$	→	 π^*_{aryl}	11%
23	228.0	0.0427	 $\pi_{\text{Ir-CO}}; \pi^*_{\text{Ir-aryl}}; \pi_{\text{aryl}}$	→	 P centred	77%
			 $d_{yz}; \pi_{\text{aryl}}$	→	 π^*_{aryl}	16%
21	224.5	0.0152	 $\pi_{\text{Ir-CO}}$	→	 $\pi^*_{\text{Ir-CO}}$	49%
			 $\pi_{\text{Ir-CO}}$	→	 $\pi^*_{\text{Ir-CO}}$	24%
			 $\pi_{\text{Ir-CO}}$	→	 $\pi^*_{\text{Ir-CO}}$	20%

19	221.1	0.1071	 $\pi_{\text{Ir-CO}}; \pi^*_{\text{Ir-aryl}}; \pi_{\text{aryl}}$	→	 $\pi_{\text{Ir-CO}}; \pi^*_{\text{Ir-aryl}}; \pi^*_{\text{aryl}}$	46%
			 $d_{yz}; \pi_{\text{aryl}}$	→	 π^*_{aryl}	33%
			 $\pi_{\text{Ir-CO}}; \pi^*_{\text{Ir-aryl}}; \pi_{\text{aryl}}$	→	 $\pi_{\text{aryl-Ir-CO}}; \pi^*_{\text{aryl}}$	16%
32	215.9	0.0371	 d_{z^2}	→	 $\pi_{\text{aryl-Ir-CO}}$	88%
34	207.0	0.0162	 $\pi_{\text{Ir-CO}}$	→	 π^*_{aryl}	93%
40	203.5	0.0334	 d_{z^2}	→	 P centred	39%
			 d_{yz}	→	 P centred	34%
			 $\rho_p; \pi_{\text{aryl}}$	→	 π^*_{aryl}	15%

29	202.1	0.4033	 $\pi_{\text{Ir-CO}}; \pi^*_{\text{Ir-aryl}}; \pi_{\text{aryl}}$	→	 π^*_{aryl}	55%
			 π_{aryl}	→	 π^*_{aryl}	36%
20	195.4	0.0510	 $\pi_{\text{Ir-CO}}$	→	 $\sigma^*_{\text{aryl-Ir-CO}}; \sigma^*_{\text{P-Ir-P}}$	95%
35	189.8	0.0415	 $\pi_{\text{Ir-CO}}; \pi^*_{\text{Ir-aryl}}; \pi_{\text{aryl}}$	→	 $\pi_{\text{aryl-Ir-CO}}; \pi^*_{\text{aryl}}$	85%
38	184.7	0.0371	 $\sigma_{\text{Ir-aryl}}; \sigma^*_{\text{Ir-CO}}; \pi^*_{\text{aryl}}$	→	 $\pi_{\text{P-Ir-CO}}; \pi^*_{\text{aryl}}$	79%
			 d_{z^2}	→	 $\pi_{\text{aryl-Ir-CO}}$	11%

2.3.3 TD-DFT analysis of **2**

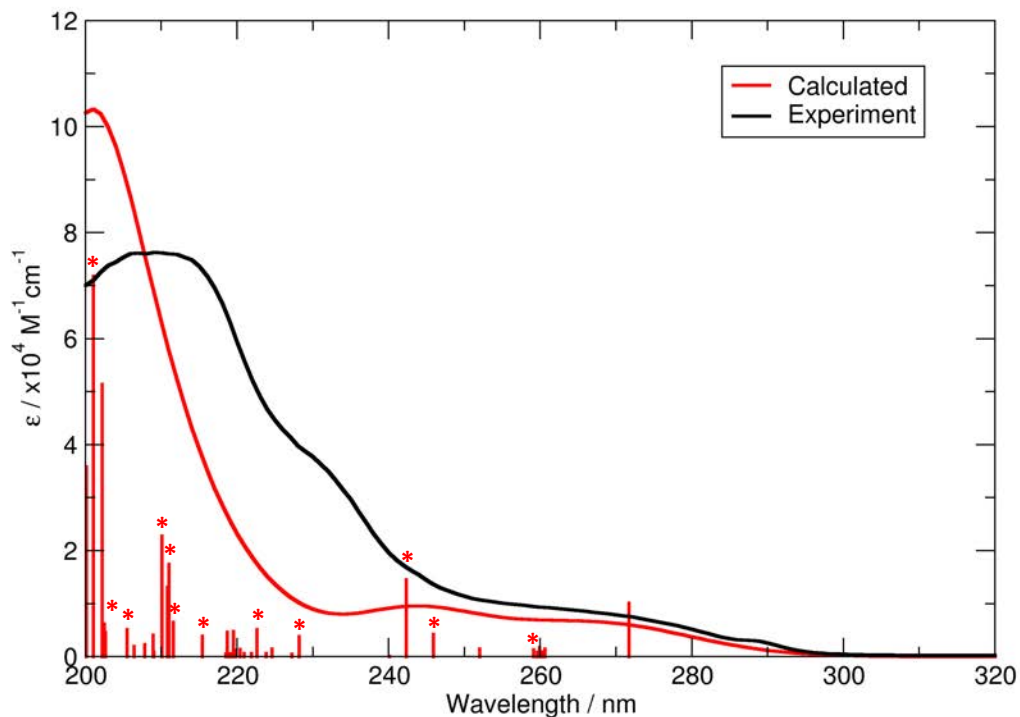
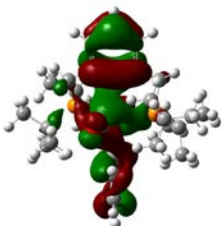
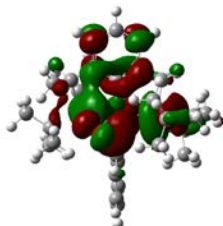
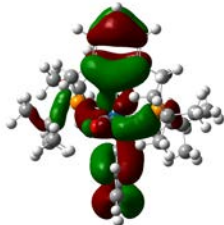
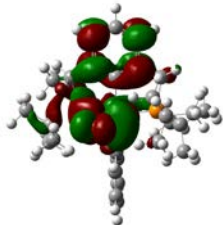
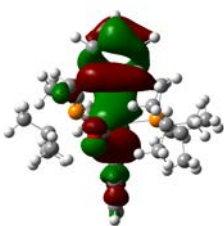
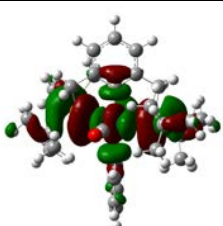
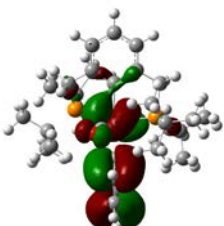
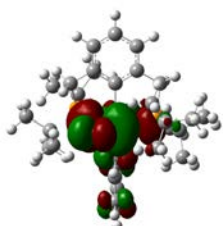
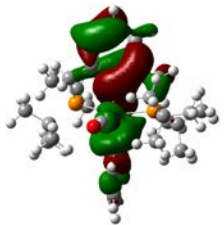
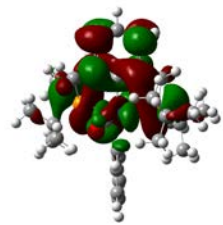
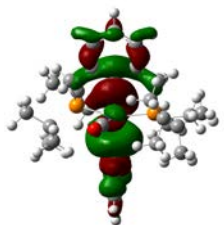
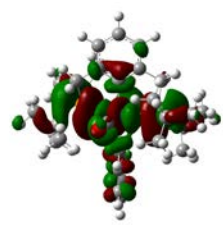
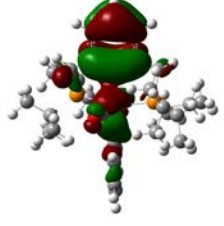
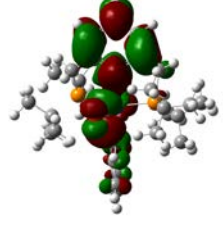
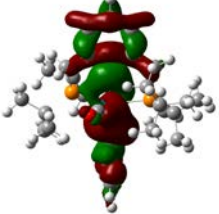
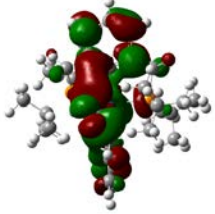
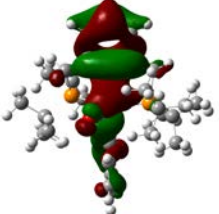
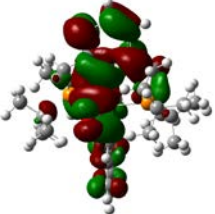
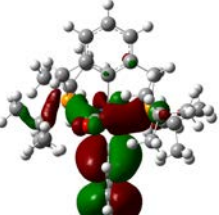
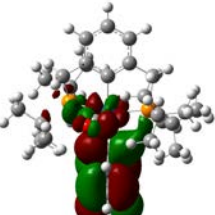
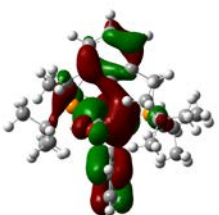
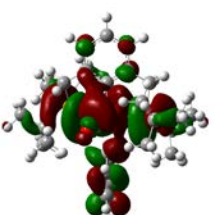
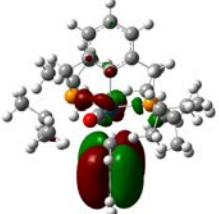
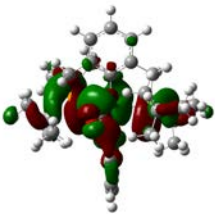
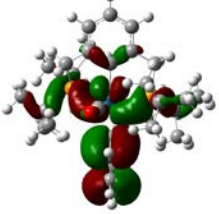
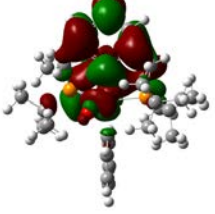
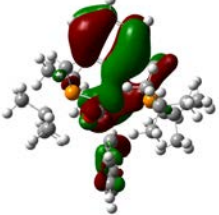
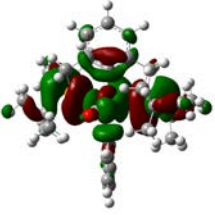


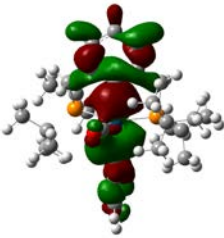
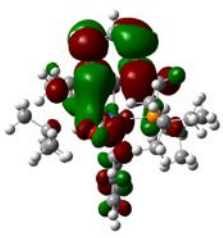
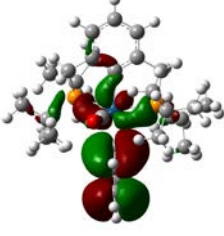
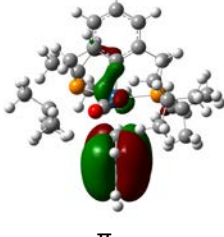
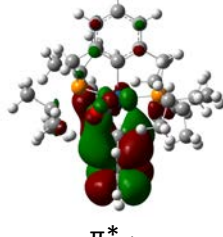
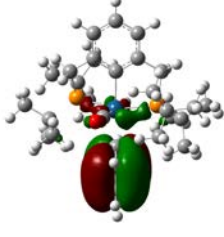
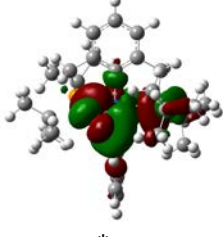
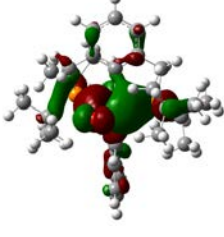
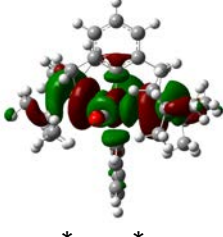
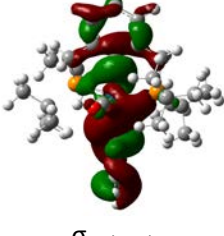
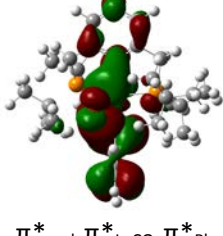
Figure S-40: Overlay of experimental and calculated UV-Vis spectra for **2**. Gaussian convolution applied to calculated vertical transitions with a FWHM of 5000 cm^{-1} . Vertical transitions depicted at an arbitrary relative intensity for graphical clarity. Excitations marked with an asterisks correspond to $\pi_{\text{M-CO}} \rightarrow \pi^*_{\text{M-CO}}$ or $\pi_{\text{M-CO}} \rightarrow \text{non-bonding}_{\text{M-CO}}$ transitions.

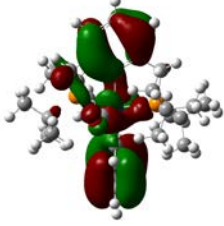
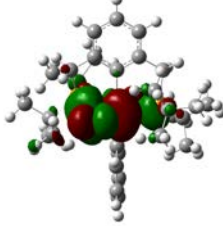
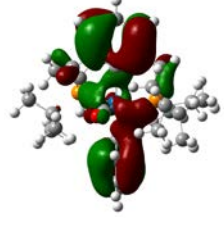
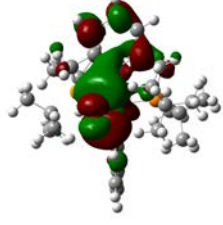
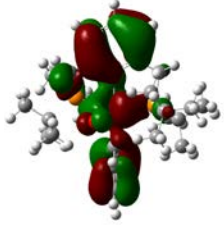
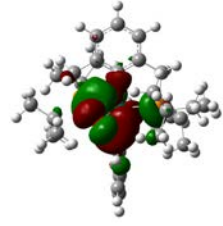
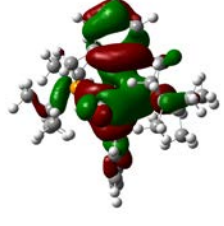
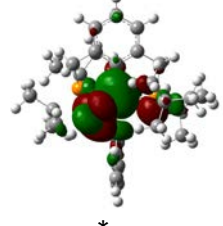
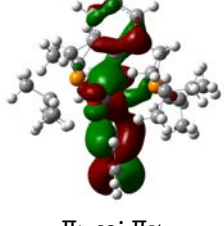
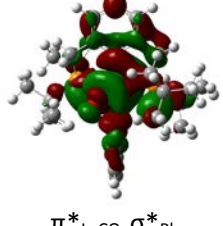
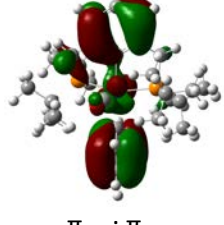
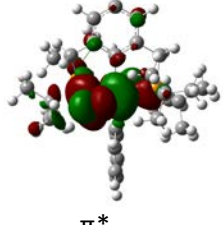
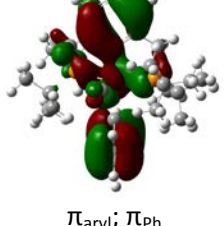
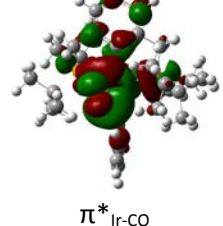
Table S-4: TD-DFT derived excitation energies for **1** restricted to those with oscillator strengths (f) greater than 0.01. Calculated NTOs with a greater than 10% contribution to a given excitation are shown rendered with an isosurface value of 0.02 and the major constituent molecular and atomic orbitals assigned.

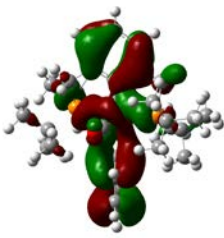
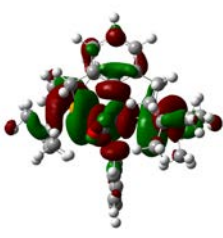
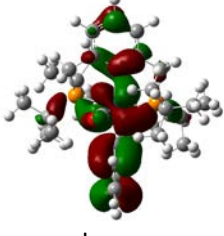
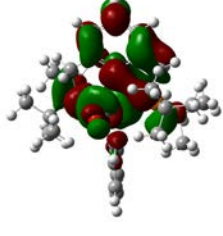
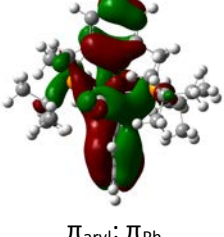
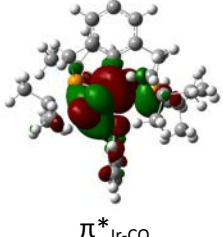
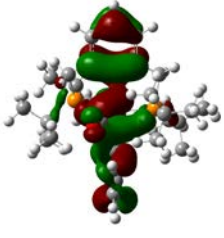
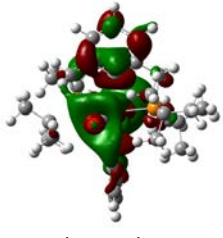
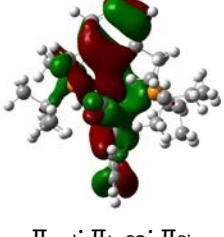
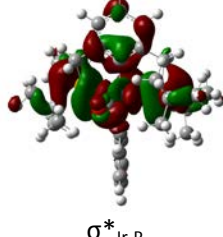
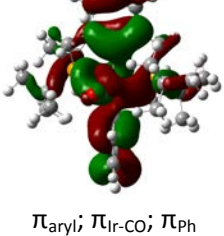
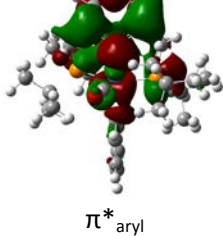
State	λ / nm	f	Contributing Natural Transition Orbitals
1	271.7	0.0685	

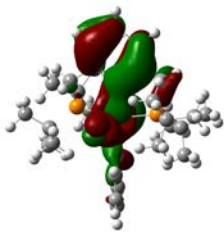
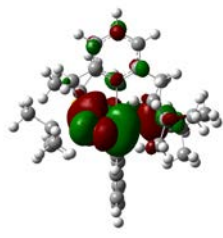
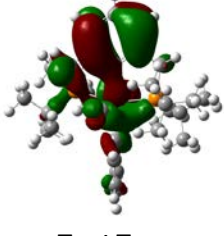
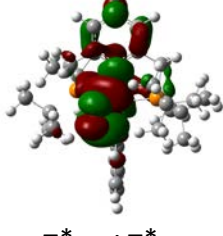
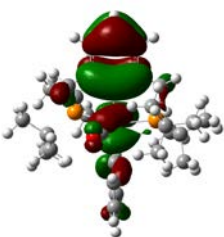
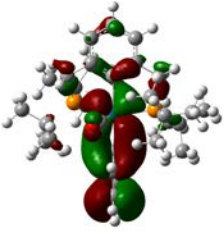
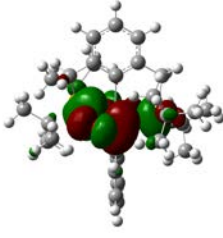
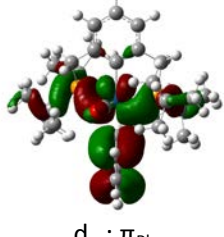
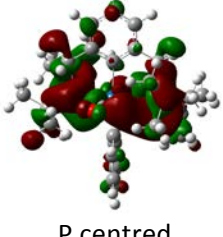
3	259.9	0.0119	 $\pi_{\text{aryl}}; \pi_{\text{Ir-CO}}; \pi_{\text{Ph}}$	→	 $\pi^*_{\text{Ir-CO}}; \pi^*_{\text{aryl}}$	70%
			 $\pi_{\text{aryl}}; \pi_{\text{Ir-CO}}; \pi_{\text{Ph}}$	→	 $\pi^*_{\text{Ir-CO}}; \pi^*_{\text{aryl}}$	16%
9	245.9	0.0285	 $\pi_{\text{aryl}}; \pi_{\text{Ir-CO}}$	→	 $\sigma^*_{\text{Ir-P}}$	55%
			 $\pi_{\text{Ir-CO}}; \pi_{\text{Ph}}$	→	 $\pi^*_{\text{Ir-CO}}$	27%
			 $\sigma_{\text{aryl-Ir-Ph}}$	→	 $\sigma^*_{\text{Ir-P}}; \pi^*_{\text{aryl}}$	12%
8	242.3	0.0983	 $\sigma_{\text{aryl-Ir-Ph}}$	→	 $\sigma^*_{\text{Ir-P}}$	78%
			 $\pi_{\text{aryl}}; \pi_{\text{Ir-CO}}$	→	 $\pi^*_{\text{Ir-CO}}; \pi^*_{\text{aryl}}$	12%

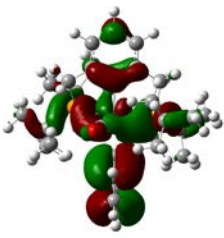
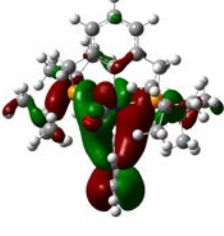
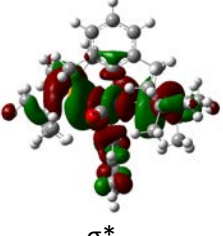
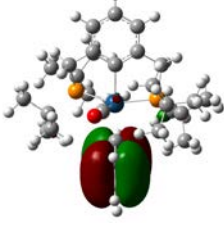
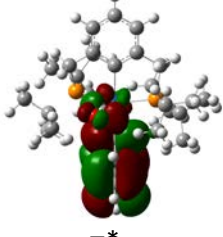
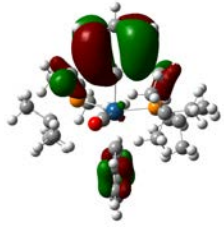
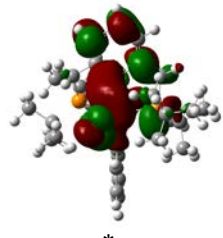
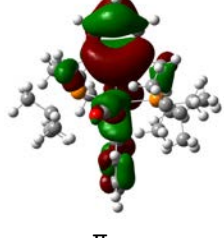
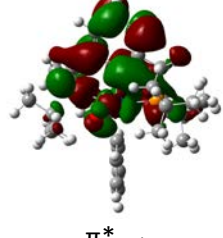
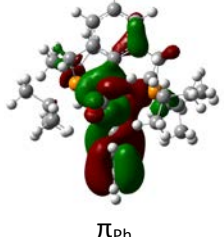
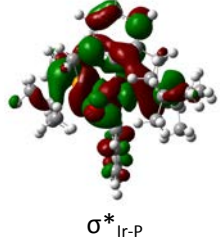
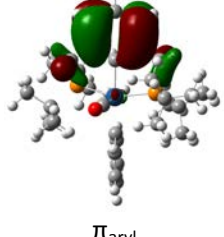
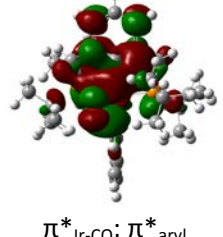
11	228.2	0.0258	 $\sigma_{\text{aryl-Ir-Ph}}$	→	 $\pi^*_{\text{Ir-CO}}; \pi^*_{\text{aryl}}$	56%
			 $\sigma_{\text{aryl-Ir-Ph}}$	→	 $\pi^*_{\text{Ir-CO}}; \pi^*_{\text{aryl}}$	14%
			 $\pi_{\text{Ir-CO}}; \pi_{\text{Ph}}$	→	 π^*_{Ph}	13%
			 $\pi_{\text{Ir-CO}}; \pi_{\text{Ph}}$	→	 $\pi^*_{\text{Ir-CO}}; p_{\text{P}}$	11%
24	222.6	0.0347	 π_{Ph}	→	 $\pi^*_{\text{Ir-CO}}; p_{\text{P}}$	89%
26	219.5	0.0323	 $d_{xy}; \pi_{\text{Ph}}$	→	 π^*_{aryl}	57%
			 π_{aryl}	→	 $\sigma^*_{\text{Ir-P}}$	34%

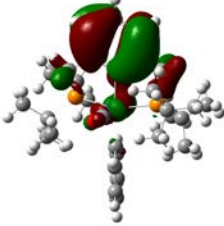
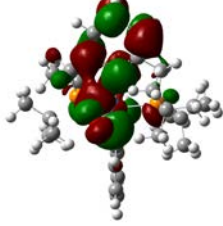
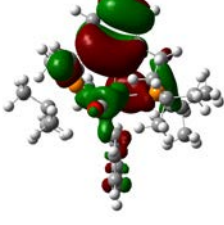
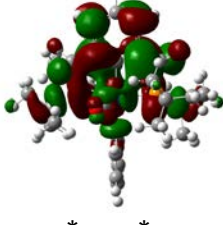
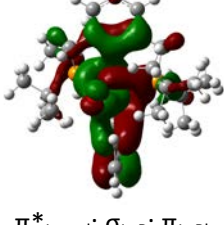
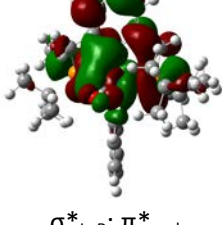
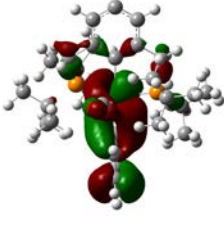
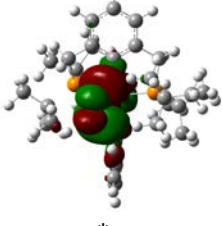
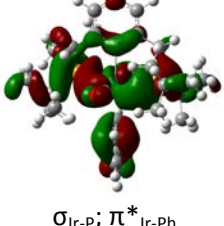
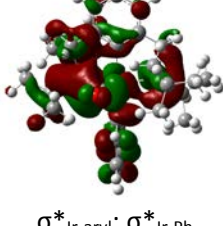
13	218.7	0.0315	 $\sigma_{\text{aryl-Ir-Ph}}$	→	 π^*_{aryl}	44%
			 π_{Ph}	→	 π^*_{Ph}	27%
			 π_{Ph}	→	 π^*_{Ph}	16%
29	215.4	0.0263	 π_{Ph}	→	 $\pi^*_{\text{Ir-CO}}$	83%
12	211.6	0.0440	 $\pi_{\text{Ir-CP}}$	→	 $\sigma^*_{\text{Ir-P}}; \sigma^*_{\text{Ir-CO}}$	76%
			 $\sigma_{\text{aryl-Ir-Ph}}$	→	 $\pi^*_{\text{aryl}}; \pi^*_{\text{Ir-CO}}; \pi^*_{\text{Ph}}$	12%

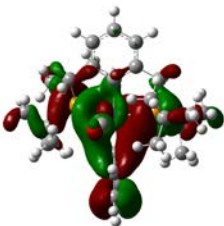
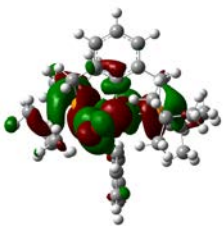
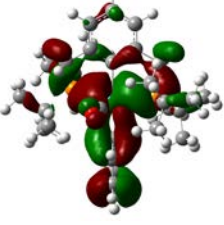
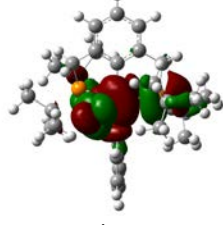
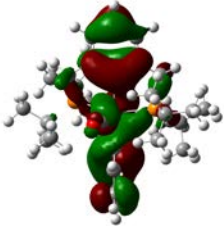
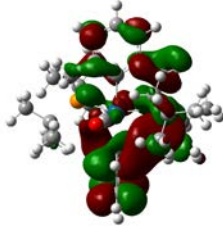
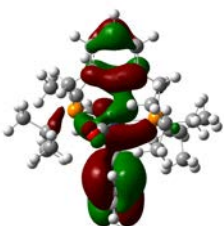
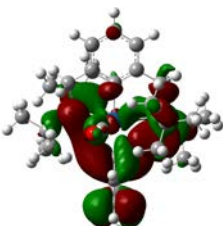
31	211.0	0.1183	 $\pi_{\text{aryl}}; \pi_{\text{ph}}$	→	 $\pi^*_{\text{Ir-CO}}$	74%
			 $\pi_{\text{aryl}}; \pi_{\text{ph}}$	→	 $\pi^*_{\text{Ir-CO}}$	15%
27	210.8	0.0887	 $\pi_{\text{Ir-CO}}; \pi_{\text{ph}}$	→	 $\pi^*_{\text{Ir-CO}}$	50%
			 $\pi_{\text{aryl}}; \pi_{\text{Ir-CO}}$	→	 $\pi^*_{\text{Ir-CO}}$	27%
			 $\pi_{\text{Ir-CO}}; \pi_{\text{ph}}$	→	 $\pi^*_{\text{Ir-CO}}; \sigma^*_{\text{Ph}}$	10%
30	210.1	0.1540	 $\pi_{\text{aryl}}; \pi_{\text{ph}}$	→	 $\pi^*_{\text{Ir-CO}}$	68%
			 $\pi_{\text{aryl}}; \pi_{\text{ph}}$	→	 $\pi^*_{\text{Ir-CO}}$	15%

28	208.9	0.0276	 <p>$\pi_{\text{aryl}}; \pi_{\text{ph}}$</p>	→	 <p>$\sigma^*_{\text{Ir-P}}$</p>	47%
			 <p>$d_{xy}; \pi_{\text{ph}}$</p>	→	 <p>$\pi_{\text{Ir-aryl}}$</p>	21%
			 <p>$\pi_{\text{aryl}}; \pi_{\text{ph}}$</p>	→	 <p>$\pi^*_{\text{Ir-CO}}$</p>	18%
23	207.8	0.0153	 <p>$\pi_{\text{aryl}}; \pi_{\text{Ir-CO}}; \pi_{\text{ph}}$</p>	→	 <p>$\sigma^*_{\text{Ir-P}}; \sigma^*_{\text{Ir-CO}}$</p>	52%
			 <p>$\pi_{\text{aryl}}; \pi_{\text{Ir-CO}}; \pi_{\text{ph}}$</p>	→	 <p>$\sigma^*_{\text{Ir-P}}$</p>	25%
			 <p>$\pi_{\text{aryl}}; \pi_{\text{Ir-CO}}; \pi_{\text{ph}}$</p>	→	 <p>π^*_{aryl}</p>	15%

34	206.4	0.0134	 $\pi_{\text{aryl}}; \pi_{\text{Ir-CO}}$	→	 $\pi^*_{\text{Ir-CO}}$	68%
			 $\pi_{\text{aryl}}; \pi_{\text{Ir-CO}}$	→	 $\pi^*_{\text{Ir-CO}}; \pi^*_{\text{aryl}}$	19%
37	205.5	0.0349	 π_{aryl}	→	 π^*_{Ph}	77%
38	202.6	0.0310	 $\pi_{\text{Ir-Ph}}$	→	 $\pi^*_{\text{Ir-CO}}$	64%
			 $d_{xy}; \pi_{\text{Ph}}$	→	 P centred	21%

			 <p>π_{ph}</p>	→	 <p>P centred</p>	56%
36	202.5	0.0418	 <p>$\pi_{\text{Ir-Ph}}$</p>	→	 <p>$\sigma^*_{\text{Ir-P}}$</p>	28%
			 <p>π_{ph}</p>	→	 <p>π^*_{Ph}</p>	10%
32	202.2	0.3483	 <p>π_{aryl}</p>	→	 <p>π^*_{aryl}</p>	58%
			 <p>π_{aryl}</p>	→	 <p>π^*_{aryl}</p>	21%
			 <p>π_{ph}</p>	→	 <p>$\sigma^*_{\text{Ir-P}}$</p>	10%
35	201.0	0.4864	 <p>π_{aryl}</p>	→	 <p>$\pi^*_{\text{Ir-CO}}; \pi^*_{\text{aryl}}$</p>	71%

33	200.1	0.2429	 π_{aryl}	→	 $\pi^*_{\text{Ir-CO}}; \pi^*_{\text{aryl}}$	45%
			 π_{aryl}	→	 $\sigma^*_{\text{Ir-P}}; \pi^*_{\text{aryl}}$	22%
			 $\pi^*_{\text{Ir-aryl}}; \sigma^*_{\text{Ir-P}}; \pi^*_{\text{Ir-Ph}}$	→	 $\sigma^*_{\text{Ir-P}}; \pi^*_{\text{aryl}}$	14%
39	197.4	0.1034	 $\pi_{\text{Ir-Ph}}$	→	 $\pi^*_{\text{Ir-CO}}$	63%
			 $\sigma_{\text{Ir-P}}; \pi^*_{\text{Ir-Ph}}$	→	 $\sigma^*_{\text{Ir-aryl}}; \sigma^*_{\text{Ir-Ph}}$	14%

40	193.8	0.4479	 $\pi_{\text{Ph}}; \sigma_{\text{Ir-P}}$	→	 $\sigma^*_{\text{Ir-P}}; \pi^*_{\text{Ir-CO}}$	34%
			 $\pi_{\text{Ph}}; \sigma_{\text{Ir-P}}$	→	 $\pi^*_{\text{Ir-CO}}$	26%
			 $\pi_{\text{aryl}}; \pi^*_{\text{Ir-Ph}}$	→	 $\pi^*_{\text{aryl}}; \pi^*_{\text{Ph}}$	15%
			 $\pi_{\text{aryl}}; \pi^*_{\text{Ir-Ph}}$	→	 π^*_{Ph}	13%

3 References

- ¹ (a) K. Krogh-Jespersen, M. Czerw, K. Zhu, B. Singh, M. Kanzelberger, N. Darji, P. D. Achord, K. B. Renkema and A. S. Goldman, *J. Am. Chem. Soc.*, 2002, **124**, 10797–10809; (b) D. Morales-Morales, R. Redón, Z. Wang, Do W Lee, C. Yung, K. Magnuson and C. M. Jensen, *Can. J. Chem.*, 2001, **79**, 823–829.
- ² C. J. Moulton and B. L. Shaw, *J. Chem. Soc., Dalton Trans.*, 1976, 1020.
- ³ J. L. Herde, J. C. Lambert, C. V. Senoff and M. A. Cushing, *Inorg. Synth.*, 1974, **15**, 18–20.
- ⁴ I. Göttker-Schnetmann, P. White and M. Brookhart, *J. Am. Chem. Soc.*, 2004, **126**, 1804–1811.
- ⁵ M. Kanzelberger, B. Singh, M. Czerw, K. Krogh-Jespersen and A. S. Goldman, *J. Am. Chem. Soc.*, 2000, **122**, 11017–11018.
- ⁶ M. J. Frisch, G. W. Trucks, H. B. Schlegel, G. E. Scuseria, M. A. Robb, J. R. Cheeseman, J. A. Montgomery Jr., T. Vreven, K. N. Kudin, J. C. Burant, J. M. Millam, S. S. Iyengar, J. Tomasi, V. Barone, B. Mennucci, M. Cossi, G. Scalmani, N. Rega, G. A. Petersson, H. Nakatsuji, M. Hada, M. Ehara, K. Toyota, R. Fukuda, J. Hasegawa, M. Ishida, T. Nakajima, Y. Honda, O. Kitao, H. Nakai, M. Klene, X. Li, J. E. Knox, H. P. Hratchian, J. B. Cross, V. Bakken, C. Adamo, J. Jaramillo, R. Gomperts, R. E. Stratman, O. Yazyev, A. J. Austin, R. Cammi, C. Pomelli, J. W. Ochterski, P. Y. Ayala, K. Morokuma, G. A. Voth, P. Salvador, J. J. Dannenberg, V. G. Zakrzewski, S. Dapprich, A. D. Daniels, M. C. Strain, O. Farkas, D. K. Malick, A. D. Rabuck, K. Raghavachari, J. B. Foresman, J. V. Ortiz, Q. Cui, A. G. Baboul, S. Clifford, J. Cioslowski, B. B. Stefanov, G. Lui, A. Liashenko, P. Piskorz, I. Komaromi, R. L. Martin, D. J. Fox, T. Keith, M. A. Al-Laham, C. Y. Peng, A. Nanayakkara, M. Challacombe, P. M. W. Gill, B. Johnson, W. Chen, M. W. Wong, C. Gonzalez and J. A. Pople, *Gaussian 03*, Revision D.02, Gaussian, Inc., Wallingford CT, 2004.
- ⁷ See for example: (a) M. Bühl, C. Reimann, D. A. Pantazis, T. Bredow and F. Neese, *J. Chem. Theory Comput.*, 2008, **4**, 1449–1459; (b) J. M. Younker and K. D. Dobbs, *J. Phys. Chem. C*, 2013, **117**, 25714–25723; (c) A. C. Tsipis, *Coordin. Chem. Rev.*, 2014, **272**, 1–29.
- ⁸ (a) P. J. Hay and W. R. Wadt, *J. Chem. Phys.*, 1985, **82**, 270–310; (b) J. P. Perdew, *Phys. Rev. B*, 1986, **33**, 8822–8824; (c) A. D. Becke, *Phys. Rev. A*, 1988, **38**, 3098–3100.
- ⁹ F. Neese, *Comput. Mol. Sci.*, 2012, **2**, 73–78
- ¹⁰ (a) K. Eichkorn, O. Treutler, H. Ohm, M. Haser and R. Ahlrichs, *Chem. Phys. Letters*, 1995, **240**, 283–290; (b) K. Eichkorn, F. Weigend, O. Treutler and R. Ahlrichs, *Theor. Chem. Acc.*, 1997, **97**, 119–124; (c) S. Grimme, *J. Chem. Phys.* 2006, **124**, 034108–1–16.
- ¹¹ S. Kossmann and Frank Neese, *J. Chem. Theory Comput.* 2010, **6**, 2325–2338.